AD-A064 299 UNIVERSITY OF SOUTHERN CALIFORNIA LOS ANGELES ELECTR--ETC F/G 20/12
EVALUATION OF GALLIUM NITRIDE FOR ACTIVE MICROWAVE DEVICES.(U)
SEP 78 M GERSHENZON N00014-75-C-0295

UNCLASSIFIED NL

1 OF 1

AD
A064 299

END
DATE
FILMED
4--79
DDC

SECURITY CLASSIFICATION OF THIS PAGE (When Data Entered)

REPORT DOCUMENTATION PAGE

READ INSTRUCTIONS BEFORE COMPLETING FORM

1. REPORT NUMBER	2. GOVT ACCESSION NO.	3. RECIPIENT'S CATALOG NUMBER
4. TITLE (and Subtitle) Evaluation of Gallium Nitride For Active Microwave Devices.		5. TYPE OF REPORT & PERIOD COVERED Annual Technical rept. AUG 77 - SEP 78
		6. PERFORMING ORG. REPORT NUMBER N/A
7. AUTHOR(s) M. Gershenzon		8. CONTRACT OR GRANT NUMBER(s) N00014-75-C-0295
9. PERFORMING ORGANIZATION NAME AND ADDRESS Electronic Sciences Laboratory University of Southern California University Park, Los Angeles CA 90007		10. PROGRAM ELEMENT, PROJECT, TASK AREA & WORK UNIT NUMBERS PE 61153N RR 021-02-03 NR 243-004
11. CONTROLLING OFFICE NAME AND ADDRESS ONR Code 427 Arlington, VA 22217		12. REPORT DATE September 1978
		13. NUMBER OF PAGES 80
14. MONITORING AGENCY NAME & ADDRESS (if different from Controlling Office)		15. SECURITY CLASS. (of this report) Unclassified
		15a. DECLASSIFICATION/DOWNGRADING SCHEDULE N/A

16. DISTRIBUTION STATEMENT (of this Report)

Approved for public release; distribution unlimited

17. DISTRIBUTION STATEMENT (of the abstract entered in Block 20, if different from Report)

18. SUPPLEMENTARY NOTES

ONR Scientific Officer
Telephone (202) 696-4218

19. KEY WORDS (Continue on reverse side if necessary and identify by block number)

annealing; photoluminescence; Gallium Nitride; epitaxy; crystal growth

20. ABSTRACT (Continue on reverse side if necessary and identify by block number)

Thick GaN crystals can now be grown (by the non-equilibrium CVD reaction of GaCl and NH_3) that are free of the precipitates, voids and microcracks that plagued us last year. However, they are still dominated electrically by a native shallow donor effect. A high pressure-high temperature system for annealing crystals and for growing crystals by liquid phase epitaxy under high pressure N_2 instead of NH_3 has been assembled and calibrated, and the first experiments begun to eliminate the native donor, so as to (over)

DD FORM 1473, 1 JAN 73 EDITION OF 1 NOV 65 IS OBSOLETE
S/N 0102-014-6601

Enclosure (2)

SECURITY CLASSIFICATION OF THIS PAGE (When Data Entered)

AD A064299

DDC FILE COPY

LEVEL II

DDC RECEIVED FEB 6 1979

79 02 02 024

361 620

prepare samples suitable for high-field electrical measurements. A survey of as-grown crystals, crystals doped during growth and ion-implanted crystals, using bound exciton and donor-acceptor, low temperature photoluminescence, has enabled us to identify many common shallow and deep donors and acceptors in GaN and to determine their ionization energies for the first time. Finally, we have excited the electron-hole liquid droplet phase in GaN and have built optically pumped ultraviolet emitting lasers based on this recombination mechanism.

Table of Contents

Introduction 1

Standard Crystal Growth by Chemical Vapor Deposition.......... 2

CVD Growth Experiments: Basal Plane Growth, Carbon Doping.......... 3

High Pressure N_2 Synthesis and Processing.......... 4

Ion Implantation.......... 14

Low Temperature, Near-edge Photoluminescence.......... 16

Electron-Hole Droplet Recombination, Stimulated Emission and Optically Pumped Ultraviolet GaN Lasers 21

Appendix: Stimulated Emission and Laser Action in Gallium Nitride.......... 24

ACCESSION for
NTIS White Section ☑
DDC Buff Section ☐
UNANNOUNCED ☐
JUSTIFICATION
BY
DISTRIBUTION/AVAILABILITY CODES
Dist. AVAIL. and/or SPECIAL
A

Introduction

GaN is a wide, direct gap III-V semiconductor, with a bandgap of 3.4eV in the ultraviolet, and which may prove to be a useful semiconductor for microwave and for electroluminescence devices. Its possible usefulness for power microwave amplifiers (high-field, transit-time controlled devices) is based upon a predicted high saturated drift velocity and upon a predicted high pair-production threshold. Taken together, these predicted values yield a figure-of-merit 20 times higher than that for Si for a fast power amplifier.

The goal of this contract has been the preparation of suitable samples to measure these two vital parameters, and, incidentally, to establish the technological base for the use of GaN in semiconductor devices. However, three problems have interfered with the achievement of these goals.

First, the melting point of GaN is in the neighborhood of 2000°C and the equilibrium N_2 pressure over such a melt may be greater than 40,000 atm. Even at 1000°, well below the melting point, the decomposition pressure is already 100 atm. The trick to growing GaN is to note that at 1000°, 100 <u>atm</u> of N_2 should be in equilibrium with 10 <u>torr</u> of NH_3. However, the homogeneous dissociation of NH_3 into N_2 and H_2 is very slow at temperatures below 1100° and so low pressures of NH_3 can be used instead of high pressures of N_2 to grow GaN well below its melting point, in our case, by its chemical vapor reaction with GaCl. During this process, the GaN slowly dissociates into Ga and N_2. Hence, the growth is basically a non-equilibrium process, where we force the formation reaction to be faster than the decomposition reaction.

Second, unless the crystals are intentionally compensated, their electrical properties are dominated by the presence of a native shallow

donor at concentrations between 10^{18} and 10^{19} per cm^3 and no low resistivity p-type material has ever been reported.

Third, GaN is normally grown on sapphire substrates. Thin crystals, less than about 30μm thick, often exhibit grain boundaries, voids, occlusions, high dislocation densities and a considerable degree of strain. These defects tend to diminish as the thickness increases. In addition, the resistivity tends to increase with increasing thickness.

In previous reports, we surmised that the native donors might be associated in some way with these defects, and so we described the rapid growth of thick (up to 5mm) crystals. However these were characterized by very heavy Ga precipitation and by the appearance of cracks and voids. Last year we described a high pressure-high temperature system that we were assembling in order to anneal GaN crysals and to grow GaN by liquid phase epitaxy using N_2 instead of NH_3 at temperatures much closer to the true melting point. The system was designed to go to $1500^{o}C$ and 10,000 atm, of N_2, so as to study and control the native donor, assuming its density to be relatable to equilibrating N_2 pressure and assuming 1500° to be high enough to allow equilibration with bulk crystals. At that time we noted that all available crystals were degenerately doped n-type by the native donor, so that the electrical properties due to intentionally added impurities could not be determined by simple Hall and resistivity measurements vs. temperature. This meant that the basic semiconductor doping parameters, which elements are donors, which acceptors, which shallow, which deep, were not known for GaN. However, we discovered a technique, low temperature, bound-exciton luminescence, which was able to detect at least two acceptors and one shallow donor in addition to the native shallow donor, unmasked by the pervasiveness of the native donor.

79 02 02 024

In this report we show that the native donor is not associated with crystal imperfections. We can now grow thick crystals on sapphire via GaCl and NH_3 that are not cracked and are relatively free of precipitates and voids. We can now grow thinner crystals (to 30μm) in which resistivity and defects no longer depend on thickness. We can grow extremely planar surfaces if we use other substrate orientations. However, in all of these, the omnipresent native donor still dominates the electrical properties.

The high pressure-high temperature system is now set up and calibrated to 1200^0 and 5,000 atm. of N_2. We have succeeded in growing GaN by liquid phase epitaxy grom Ga and N_2 and have started to anneal previously grown specimens at these high N_2 pressures. It is still too early to tell whether we can affect the native donor by these treatments.

We have doped CVD grown GaN crystals by ion implantation or by doping during growth with a wide selection of elements predicted to be shallow donors and shallow acceptors, or to be expected as common impurities. This was done partly to establish a semiconductor technology for GaN - what are the shallow donors and acceptors - and partly in an attempt to compensate or otherwise affect the native donor. The low temperature photoluminescence experiments extended to these materials have now provided us with a wealth of information about these doping elements, not only from bound-exciton luminescence, but also from donor-acceptor and free-to-bound transitions. We have now determined for the first time which elements are shallow donors and which shallow acceptors in GaN, what their ionization energies are, and also which elements give rise to deep levels.

During the photoluminescence experiments, we discovered a broad emission band which dominated the spectra at the highest excitation intensities. This band exhibited stimulated emission gain. By analyzing this band (spectra, excitation dependence of spontaneous and stimulated emission, dependence on

excitation volume, temperature dependence) we were able to show that the emission was due to formation of electron-hole liquid metallic droplets. We were able to work out the phase diagram of this electron-hole liquid and to show that this phase is stable to over $80^{o}K$, the highest stability of such a phase in any material. By preparing good optical cavities in several crystals we were able to make ultraviolet lasers via this recombination mechanism using optical pumping. Finally, from threshold and gain-loss measurements on such lasers, we were able to show that the losses determined indicate that these GaN crystals are of good semiconductor quality, despite the presence of the native donor.

The net result of our progress this year is the realization that it is only the native donor that stands in the way of our making definitive drift velocity and pair production measurements and of utilizing GaN as a "normal" semiconductor. But now perhaps, we have the tools to alter the native donor density (high pressure N_2 at high temperatures) and the means to measure it (low temperature photoluminescence).

Standard Crystal Growth by Chemical Vapor Deposition

Our previous reports have described the slowly improving quality of GaN grown epitaxially on sapphire by the CVD reaction of GaCl and NH_3 at about $1050^{o}C$. Our early results indicated that the most rapid growth occurred on R-plane ($\bar{1}012$) substrates, although the surface growth morphology was not planar. We learned how to clean the sapphire (H_2 at 1200°) to avoid an extra slow-growth stage required during nucleation. We learned how to minimize contamination in the 10^{19}-$10^{20}cm^{-3}$ range due to Si, a shallow donor, by using an alumina liner in the furnace to eliminate contact with

the fused silica envelope and by using higher purity starting materials. The electrical properties were now dominated by an always-present shallow donor, 2-5 x $10^{18} cm^{-3}$, which we showed to be a native defect by eliminating any association between it and any expected contaminant in that concentration range. Since the bulk resistivity of the crystals increased with thickness, we surmised that this donor might be due to growth related imperfections which decreased with thickness, and we began a program to grow very thick crystals. By optimizing the temperature profile, the flow rates, substrate placement and flow geometry, we were able to grow GaN single crystals on 2x2cm R-plane sapphire up to 10mm thick. Last year we set up a second CVD apparatus to grow such thick crystals routinely. Last year we also reported that such rapidly grown thick crystals were characterized by three types of defects: (1) a pervasive precipitation of very small (< 100 Å) Ga particles, (2) large voids frequently containing free Ga and usually oriented on crystallographic planes, and (3) microcracks on crystal cleavage planes, starting from the uppermost surface, but seldom passing through the entire thickness of the epitaxial GaN layer. These defects lead to catastrophic breakdown even in very modest electric fields (10^3 -10^4V/cm), and aborted our attempted measurements of the high field drift velocity.

This year, we have therefore devoted a major effort in an attempt to understand the origin of these defects in order to eliminate them. Our tools have been optical microscopy, scanning electron microscopy, transmission electron microscopy and back-reflection Laue x-ray diffraction.

First we consider the cracks. The coefficient of thermal expansion of sapphire is larger than that of GaN. Thus on cooling the newly grown crystal from 1050°C to room temperature, the sapphire shrinks more than the grown crystal and therefore, the sapphire should be in tension, the GaN in compression. Hence it is the sapphire that should crack, not the GaN.

In fact, the sapphire does crack. Whenever the GaN layer thickness is greater than about 70μm, the sapphire substrates always exhibit cracking and crazing extending completely through their thickness. It is observed that the GaN does not crack at all unless its thickness is at least 200μm and then the microcracks formed radiate from the top surface, rather than from the interface with the sapphire and these usually do not propagate all the way through to the interface. A very simple and straight-forward stress analysis shows why the GaN cracks even though it should be under compressive stress. The differential strain arising at the interface results in a bending moment with the outer surface of the GaN being bowed into a convex form. Although the stress in the GaN is compressive at the interface, the bowing causes it to slowly change to a tensile stress at the outer surface and this stress, maximum at the outer surface, increases for thicker cyrstals where the bending (bowing) moment increases. This then qualitatively explains why the thick layers (> 200μm) exhibit microcracks and why these originate at the outer surface, rather than at the interface. Quantitatively, the calculated minimum tensile force which causes cracks to appear at the onset 200μm thickness due to differential thermal contraction of the GaN-sapphire sandwich from 1050° to room temperature is about two orders of magnitude less than the predicted ultimate fracture strength of an ideally perfect GaN crystal. Thus the cracks should originate at locallized crystallographic defects. In fact, this is exactly what is observed. The cracks all originate at the upper GaN surface and always pass through one or more of the large voids (discussed below) lying on or just below the surface. Thus, to grow crystals thicker than 200μm, growth should be interrupted prior to attaining this thickness. The sapphire substrate should then be removed (chipped and ground off) and growth resumed

without the presence of the GaN-sapphire interface. In fact, this procedure does work and very thick crystals can be grown without the associated microcracks. However, as noted below, the original motivation for growing very thick crystals (the increase in resistivity with thickness) is no longer operative. For relatively pure crystals, primarily low Si contamination, the resistivity no longer increases with thickness, as long as the thickness is greater than 30-50μm.

The second problem associated with the rapid growth of thick GaN crystals on R-plane sapphire is the frequent occurrence of large voids, often containing some free Ga. We have now shown that this feature is associated both with the substrate orientation and with the fast rate of growth. The best lattice match between GaN and R-plane ($\bar{1}012$) sapphire is the ($11\bar{2}0$) prism plane of GaN and the GaN does exhibit that orientation, with its c-axis in the plane of growth oriented parallel with the projection of the sapphire c-axis in that plane. This GaN prism plane is a very slow growth plane, and unfortunately, the fast growth planes are not perpendicular to it. The latter lead to the development of other (slow-growing or "equilibrium") facets which are predominantely R-planes ($\bar{1}012$) or R-like planes ($\bar{1}01n$) with smaller angles between the plane and the c-axis. This results in a non-planar surface morphology. The surface consists of a series of ridges bounded by these R-like planes. During the initial growth stage, many nuclei form, each bounded by such planes. As the nuclei grow and merge, these form a very large number of small ridges and valleys and the many re-entrant boundaries in the valleys allow rapid growth to occur. As growth progresses, the ridges tend to become fewer in number presumably due to slightly different growth rates in adjacent valleys. As the ridges merge, the R-like facets become larger and the number of re-entrant edges decrease, the latter resulting in a decreased over-all growth rate. In addition, prism plane (slow growth) facets begin developing from the edges of the crystals, again

decreasing the number of re-entrant edges and decreasing the growth rate. Thus, for thick crystals, the growth mechanism changes. The slow growing R-like planes become the dominant growth planes. These planes grow with different growth velocities. Thus, for a ridge which is the intersection of two different planes of this type, one side of the ridge grows faster than the other side. This leads to the development of "overhanging cliffs". Continued growth extends these overhangs into cave-like structures, which sometimes get covered over, forming cavities. These are the large gross voids we observe. Once the cavity is formed, it is no longer in contact with NH_3 and the GaN slowly deocmposes into Ga and N_2 leaving free Ga in the voids. This problem then is associated with the appearance of well developed large area facets as the crystals become very thick. For thick crystals the problem cannot be eliminated, but it can be minimized by slowing the growth rate down and supplying excess NH_3 as the crystals get thicker. This slows the growth of the overhangs and allows the valley growth to keep up with ridge growth and avoid the formation of caves. At over-all growth rates of 60μm/hr, this becomes a problem when the crystals are only 30μm thick. At 30μm/hr void-free crystals can be grown to 60μm thicknesses, and for very slow growth rates, 1-10μm/hr, crystals at least 200μm thick can be grown without such voids. Again, note that we no longer desire to grow crystals thicker than about 60μm.

The last major defect of our standard CVD grown crystals on R-plane sapphire is the appearance of a mist of very small Ga precipitates (<100 Å) scattered throughout the volume of the crystal. These scatter light and render the thicker samples completely opaque to transmitted light. These defects are also associated with growth rate. In our CVD system the growth rate is directly related to the GaCl flow rate (HCl over Ga at 950°)

not to the NH_3 flow rate. For rapid growth of very thick crystals we increased the Ga transport rate, not the NH_3 flow. Hence, it is not surprising that under such conditions free Ga forms on the growing surface and gets incorporated into the growing crystal before it can react with NH_3. We should be able to avoid this disproportionation by increasing the NH_3 flow rate, but in the apparatus we now have we are already working close to its maximum through-put rate for NH_3. Hence we should decrease the Ga flow rate and thus the growth rate. This does indeed work. Crystals grown at growth rates between 1 and 20μm/hr are free of such precipitates. Note that such lowered growth rates are also needed to reduce the voids discussed above.

Thus we are now able to grow very thick GaN layers, greater than 200μm, on R-plane sapphire. A two-step process (removing the sapphire) eliminates the microcracks and slow growth eliminates the precipitation and greatly reduces the number of voids. These are now good single crystals, without grain boundaries or other gross defects. The only structural defects that can be observed are microscopic basal plane stacking faults.

Since Si was removed as the major electrically-active impurity two years ago, the resistivity of the GaN no longer increases with thickness once the samples are 10-30μm thick and it is only the native donor which controls the carrier density. Thus we no longer have the impetus to grow very thick crystals, even though we are now able to do so. Our second CVD apparatus for the routine growth of GaN on R-plane sapphire now produces such uniform crystals consistently at a growth rate of 20μ/hr.

Finally, we note that the removal of all the defects discussed above had no effect on the presence of the native donor. The native donor density in the routinely grown crystals is 10^{18}-10^{19} cm^{-3} and the mobility is consistently about 100 cm^2/V-sec.

CVD Growth Experiments: Basal Plane Growth, Carbon Doping

Two years have now passed since we made the decision to concentrate on CVD growth on R-plane sapphire. Growth on that sapphire orientation yielded the fastest growing crystals. Since then, we have learned how to best clean the substrate surface, how to eliminate Si contamination, how to avoid cracks, voids and precipitates and the optimum conditions of temperature, flow rates and sample placement geometry, to produce good crystals. With this information, and knowing that many of our R-plane growth problems were associated with the resultant non-planar surface growth morphology, we decided to re-investigate CVD growth on other sapphire orientations. Avoiding the conditions that normally result in precipitation and microcracks, we found that of several orientations tried, basal plane sapphire gave excellent results. Basal plane GaN grows on basal plane sapphire. Nucleation forms islands with basal plane surfaces. These eventually merge when these islands are at different heights, producing a planar, but stepped, surface morphology. Good growth proceeds and the morphology does not change. Growth rates of 30-60μm/hr produce good crystals as defect free as the best R-plane grown crystals and the morphology is planar. The planar surfaces, free of voids and overhangs, allow us to avoid grinding and etching steps for preparing samples for electrical measurements. The native donor density (10^{18}-10^{19}cm^{-3}) and mobility is identical with those in R-plane grown samples. Thus we will now be growing basal plane GaN as well as GaN on R-plane sapphire in our standard CVD growth apparatus. So far, the only disadvantage of this is that basal plane sapphire substrates cost three times as much as R-plane wafers.

Last year's Progress Report described our initial attempts at using low temperature near gap photoluminescence to characterize impurities in as-

grown GaN. One emission line was tentatively identified with carbon on the basis of circumstantial evidence: carbon should be an expected impurity and the line was enhanced whenever graphite was used in the growth apparatus. (This identification is confirmed this year via the ion-implantation results given below.) The photoluminescence line was identified as a bound exciton line, but its energy was too low to assign it as either a shallow donor or as a shallow acceptor. Thus it had to be relatively deep. From naive chemical arguments (covalent radius, electronegativity) we suspected that, as a simple, isolated, substitutional defect, carbon should appear on a N site rather than on a Ga site, and thus act as an acceptor. We were looking for simple, easily handled acceptors, to compensate the native donor always present in our crystals. Carbon had the advantage that it was easily compatible with our CVD growth method. Thus we decided to dope our standard crystals during growth by introducing a metered flow of CH_4 into the reactor as a source of carbon. The photoluminescence of these samples showed a strong increase in the line already tentatively identified as carbon, showing that the identification was correct. However, the native donor density did not exhibit any gross changes as determined by its bound exciton spectra, nor was there any change in the shallow donor concentrations, as measured by the free electron Hall coefficient at room temperature. However, there was an unexpected increase of the electron mobility from about 100 cm^2/V-sec to almost 300 cm^2/V-sec. From the bound exciton spectra, carbon cannot be a shallow donor or a shallow acceptor. If it is a deep acceptor it should either compensate the native donor, leading to a lower free electron concentration and a lower mobility, or, if a chemical mass action equilibrium is operative at the growth temperature, it should enhance the shallow donor density, but decrease the mobility. If carbon is a deep donor it should either not affect the native donor nor the room temperature

mobility, or if a chemical mass action equilibrium occurs, it should decrease the native donor density leading to a lower electron density at room temperature but a higher mobility. None of these four possibilities agrees with the experiments. It is as if carbon were neither a donor nor an acceptor, but simply gettered the crystal, improving the mobility. If so, the luminescence line could not be due to a point defect. Rather the carbon would have to be part of an extended defect - perhaps if it is basically an acceptor, paired with the native donor to yield an electrically neutral isoelectronic center. Although carbon does not lead to lower carrier densities, its role as an enhancer of mobility is intriguing and is being pursued further.

High Pressure N_2 Synthesis and Processing

The central theme of our program now is aimed at eliminating or at least reducing the native shallow donor defect, perhaps a nitrogen vacancy. Our approach is to grow crystals or to anneal CVD grown crystals under varying pressures of N_2 rather than NH_3 and at temperatures that are sufficiently high to allow rapid diffusion and equilibration. Under such conditions, >1100°, NH_3 is no longer stable.

During the past year we have received the components of the high pressure-high temperature system that was ordered last year. This consists of a high pressure gas compressor (14,000 atm), two internally heated vessels capable of sustaining 1400°C at 10,000 atm and an externally heated vessel (1100° at 4,000 atm). These are in addition to a 3,000 atm compressor we already had.

The system was installed with its auxiliary equipment, tested section by section and then together. The experiments were delayed, originally by

malfunctions due to shipping damage, manufacturers' errors and our unfamiliarity with this equipment, and later by problems arising out of contamination of gas, gas leakage in the vessels and in the compressor, corrosion of parts due to contamination, failure of the compressor due to gas scouring of the compression cylinders and other miscellaneous "bugs".

In the first experiments, the externally heated pressure vessel was used to anneal CVD grown GaN crystals at temperatures between 800° and 1030° and N_2 pressures up to 3,000 atm. Care was exercised to remove oxygen and water vapor from the ambient. These experiments had two purposes: to deduce an accurage pressure-temperature phase diagram for the three-phase GaN-Ga-N_2 system to predict conditions for high pressure synthesis and annealing, and secondly, to begin studying the direct effects of high pressure N_2 anneals.

SEM analysis of the GaN surfaces before and after annealing provided no evidence of whether or not the samples were dissociating, since similar features appeared on the surface irrespective of whether the annealing was done well above or well below the estimated equilibrium pressure. Low temperature photoluminescence experiments showed no marked change in the shallow donor density due to annealing. These negative results in these early experiments at relatively low pressures and temperatures are not unexpected. They were designed to give us experience with the use of the equipment and with the surface effects on GaN crystals while the equipment was being tested and calibrated into its much higher pressure and temperature regimes.

Recently, experiments were begun in one of the two internally heated vessels at higher pressures, taking precautions to preclude contamination by O_2 or H_2O. A fused silica crucible containing Ga and occasionally a sapphire substrate or a CVD grown GaN crystal is placed in the furnace. After

applying N_2 pressure (4,000 to 8,600 atm) the furnace is raised to the annealing or growth temperature (960-1180°) held there for 3-8 hours, then rapidly cooled and depressurized. The Ga melt surface was invariably covered with a brittle crust containing sharply faceted crystallites ($\sim$10μm in size) and a large number of whiskers as seen by SEM and optical microscopy. The surfaces of the sapphire substrates were covered by a uniform but thin layer (10-20μm) of faceted crystal. The areas of the samples were too small for good x-ray identification or clear-cut electrical characterization, but energy dispersive analysis in the SEM indicated that Ga is the dominant constituent (N is not detectable) with Si and Al as trace contaminants. So far the electrical measurements indicate high resistivity (which is what we are seeking), but on these thin polycrystalline layers this could be due to the grain boundaries. SEM analysis of GaN grown on CVD GaN substrates did not indicate unequivocal features that could be attributed to either growth or dissolution of the substrate. Therefore separate experiments are now being done to characterize the surface of CVD grown substrates etched by dissolution at low pressures and in contact with Ga to catalyze dissolution.

Preparations are now being made to grow GaN from a Ga solution of N_2 with the solution in a thermal gradient.

Ion Implantation

GaN is invariably heavily doped n-type with 10^{18}-10^{19} native shallow donor defects per cm^3. At room temperature these are all ionized yielding a corresponding concentration of degenerate free electrons. Thus the Hall coefficient is independent of temperature. We have shown previously that Si is also a shallow donor and that if care is not taken during growth, Si will appear and enhance the already considerable electron density.

In order to intentionally dope GaN, either to compensate the native donor electrically or to depress it via a chemical mass action law effect, or to try to grow p-type material, one would like to identify the elements that are donors or acceptors, shallow or deep, perhaps their solubilities, diffusion coefficients, etc. But this information cannot be obtained from simple doping experiments followed by Hall measurements because of the dominance of the native donor. From the literature, it is known that Zn and Mg can somehow compensate GaN, but Zn-doped material sometimes comes out n-type, sometimes high resistivity, with no simple theory explaining the difference. Thus we wished to examine the behaviour of a number of chemical elements simply to identify their electrical activity in GaN. Last year we showed that we could determine their behaviour even in the presence of the native donor by using the results of near bandgap low-temperature photoluminescence. Photoluminescence is excited in GaN by a N_2 laser and the penetration depth of the excitation is only ∿2000A. Hence ion implantation, which deposits dopants in a range of this order or somewhat greater is an ideal way to dope GaN for such measurements. Further, from the fluence and the ion energy, the dopant profile is easily deduced. The only problem remaining is to anneal out the damage caused by the high energy particles and "activate" the centers.

In pure as-grown CVD GaN, the dominant near gap luminescence is due to an exciton bound to the neutral shallow native donor. After implanting with Ar^+ this luminescence disappeared. By studying the recovery of this band vs temperature and time of annealing (in flowing NH_3) it was found that a 3 hour anneal at 1000°C reproduced the original intensity. Furthermore, when other implants were done producing other luminescence features, these annealing conditions invariably optimized the emission intensity. Thus,

the annealing procedure was established.

The ion implanted samples we report here were implanted for us by Hughes Research Laboratories (with our gratitude to Dr. L. Anderson). These include C^+, Si^+, Ge^+, Sn^+, Be^+, Mg^+, Zn^+, Cd^+, O^+, S^+, Li^+, Na^+, H^+, N^+ and Ar^+. Several fluences were used for each dopant spanning the 10^{18}-$10^{20}cm^{-3}$ predicted concentration range at the peak maximum and energies were chosen to produce ranges of 2000 to 3000 Å.

Low Temperature, Near-edge Photoluminescence

Although our primary thrust this year has been towards processing GaN at high temperatures and high N_2 pressures in order to gain some control over the ubiquitous native shallow donor, most of the year has been spent setting up, testing and calibrating the new system and data is only now beginning to be obtained. However, we were fortunate in that our program to characterize donors and acceptors in as-grown CVD crystals, in crystals doped during growth and in ion implanted samples by the use of low temperature photoluminescence spectra has provided us with a wealth of new information and this in samples where the native donor masks all other impurities, at least to electrical measurements.

The spectra were recorded on a Perkin-Elmer E-1 f/8 spectrometer with an RCA 1P28 photomultiplier, using boxcar integration to improve the signal-to-noise ratio. Excitation above the band gap was by a pulsed N_2 laser (3371 Å, 10^5 W peak power, 10 ns pulses, 100 pps) focussed onto the sample immersed in liquid He. Estimating a lifetime of $\sim 10^{-10}$sec, we deduce a bulk excitation rate of 4×10^{27} electron-hole pairs / cm^3 / sec and a steady-state free carrier excitation density of $\sim 10^{17}cm^{-3}$.

The interpretation of the results is strikingly similar to those for the II-VI compound CdS and follows very closely the pioneering experiments in CdS of Thomas and Hopfield, Wheeler and Dimmock, and Reynolds and co-workers. In fact GaN and CdS are quite similar. Both are wurtzite structures with high ionicity and both have very similar electron and hole effective masses. Only their bandgaps are different.

Previous work has measured the band gap of GaN by absorption, and two of the three expected free excitons by reflectivity, and the lowest energy free exciton has also been observed in luminescence. Infrared reflectivity of the coupled plasma-reststrahlen system yielded an electron effective mass of 0.2, but a hole mass of about unity is arrived at only by naive estimation.

From the bandgap at 4.2^{o}K (3.503 eV) and the electron mass (the hole mass being much larger is therefore unimportant) the binding energy of the lowest free exciton is calculated to be 30 meV and the measured value is 28meV. From the free carrier masses and the static dielectric constant we expect the ionization energy of the shallowest (effective mass) donors to be 30 meV and the shallowest acceptors to be 150-300 meV. We expect most transitions to be replicated at lower energies by the simultaneous emission of LO phonons (90 meV). We also expect a Haynes Rule constant of 0.1 to 0.2 relating the binding energy of an exciton bound to an neutral donor or acceptor to the ionization energy of that donor or acceptor.

We start our analysis by considering the emission within 300 Å of the band edge from a series of CVD GaN crystals not intentionally doped and grown under conditions where Si contamination is low, so that the electrical properties are completely dominated by the native shallow donor (10^{18}-10^{19} cm^{-3}). More than a dozen emission bands are observed. Several of them are clearly 90 meV LO phonon replicas of other bands. The highest energy band

at 3.4751 eV is present in most samples. It coincides with the predicted lowest free exciton and agrees with that interpretation from previous reflectivity spectra. Next come two lines 3.4710 and 3.4691 eV close to the predicted position for the decay of an exciton bound to a neutral, shallow, effective mass donor. (These would be called I_2 lines in CdS). Two other, but much weaker lines at lower energies, are associated with each of these two bound excitons. As in CdS, we assume that these extra lines are due to bound exciton decay at a neutral donor, but that the final state of the transition leaves the neutral donor in an excited state. We note that the extended excited states of a donor are much more effective-mass like than the compact ground state which may deviate from its effective mass description by the so-called central-cell corrections. Hence, we assume that the two excited states we observe for each donor can be described by a simple Rydberg series corresponding to the n=2 and n=3 states. From the difference in energy between these two lines for each donor we obtain a value of the electron effective mass of 0.2, in agreement with our predictions. Finally, the difference between the n=2 and the non-hydrogenic n=1 ground state, when added to the Rydberg difference between $n=\infty$ and n=2 gives us the ionization energy of each of the donors. The results then define the two donor ionization energies: 34 meV (very close to the expected ideal effective mass value of 30 meV) and 50 meV. (We will show below that the first is the native shallow donor and the second is Si.) Both of these results produce a consistent value of 0.12 for the Haynes Rule constant relating the exciton binding energy to the donor ionization energy.

Next, at lower energies we observe two bands (3.457 and 3.455 eV) in the vicinity of the predicted position for excitons bound to shallow neutral acceptors. (These would be I_1 lines in CdS). The intensity ratio between these lines varies from sample to sample indicating that two independent

acceptors are involved, but the lower energy line is usually much stronger. No excited state replicas are observed. Hence we cannot deduce the ionization energies directly.

At yet lower energies we observe a very broad oscillatory emission complex which is simply a single broad band strongly replicated by the emission of 1, 2, 3, 4, 5 and 6 LO phonons. This structure and its position is the signature of a donor-acceptor pair band. An electron trapped on a donor recombines radiatively with a hole on an acceptor yielding an emission energy $E = Eg - (E_D + E_A) + e^2/\varepsilon r$. Here r is the separation between the donor and the acceptor and ε is the static dielectric constant. From the statistics of the pair distribution based on the known native donor concentration and from the overlap of the donor and acceptor wave function determined by the Bohr radius of the ground state of the shallow native donor, we estimate the peak of the emission should correspond to a pair separation r between 100 and 200 Å.

Next we repeat the experiment at 77°K. Here we expect the shallow donor to be ionized. Thus the recombination involves a free electron in the conduction band recombining with a hole on the acceptor. Then, comparing the 77° and 4.2^{o} results and using the known bandgap variation with temperature, the mean kinetic energy of a free electron at 77° and an average donor ionization energy between the two shallow donors for E_D, we deduce that the acceptor binding energy (the deeper acceptor of greater intensity) is 202 meV and that the coulombic term in the pair recombination energy is 11 ± 1 meV, corresponding to a pair separation at peak intensity of 140 Å (again close to the CdS value). From this acceptor energy and the position of the deeper acceptor bound exciton line we conclude that the Haynes Rule constant for acceptors is 0.1 Hence the shallower acceptor has an ionization energy of

175 meV. We will show below that the deeper acceptor is Zn or Cd (both have nearly identical binding energies) and the lower intensity acceptor is probably Ge.

Note that we now have a consistent picture establishing the Haynes Rule constants for both donors and acceptors, with the data being internally self-consistent and within the limits of the theoretical predictions.

Now we turn to the doped samples. All of these samples always exhibit the 3.4710 eV bound exciton corresponding to a donor ionization energy of 34 meV. This must be the shallow native donor which dominates all our samples in Hall and resistivity measurements.

We have previously shown that Si was also a shallow donor and that it was the dominant impurity in all our early CVD grown crystals. Thus, comparing the spectra from these early crystals, with those from the low Si later crystals, and with samples ion implanted with Si, we can identify the second bound exciton peak at 3.469 eV with a Si donor whose ionization energy is 50 meV.

Continuing with the other ion implanted samples, one by one, using the Haynes Rule constants already derived, and observing donor-acceptor pair band shifts between different acceptors and donors and high temperature free electron transitions, we deduce that both Zn and Cd are shallow acceptors with identical binding energies of 200 meV. Ge is both a donor and an acceptor with a donor energy of 67 meV and an acceptor binding energy of 175 meV. S, C, O, Mg, Be are relatively deeper levels where Haynes Rule should no longer be applicable. We wish to complete higher temperature experiments (free-to-bound transitions) before concluding whether these are donors or acceptors and what their binding energies are. Samples ion implanted with Sn, Li, Na, H and N are also being analyzed currently.

Thus, the photoluminescence data of as-grown, doped during growth, and ion implanted samples, when completed, should give us a comprehensive picture of the electrical behaviour of all simple doping elements in GaN in spite of all samples being electrically masked by the native shallow donor. In addition, this method allows us to easily monitor the native shallow donor and may, via Zeeman and stress splitting experiments shed more light on the physical structure of the native defect itself.

Electron-Hole Droplet Recombination, Stimulated Emission and Optically Pumped Ultraviolet GaN Lasers

To investigate the excitation dependence of the photoluminescence described above, the nitrogen laser was focussed to a very small spot on the samples. At these very high pump densities, a new very broad emission band was observed at energies just below the position of the shallow bound exciton lines. This band was observed irrespective of the specific sample doping. At the highest pump densities it dominated the extrinsic spectra and it exhibited line narrowing with increased excitation, characteristic of stimulated emission. Because the emission consisted of both spontaneous and stimulated components occurring simultaneously and making it impossible to sort out the spectra, we decided to study the gain characteristics separately. To do this we needed a reasonable optical cavity. As noted earlier, the surface morphology of the standard CVD crystals grown on R-plane sapphire is not planar. Rather than remove the sapphire from such samples, polish, etch and cleave them, we decided to use some of the small very planar platelets of GaN that frequently appear during CVD growth, nucleating on the tip of the NH_3 inlet tube. In the first experiments a one-sided cavity was formed. A single end mirror was fashioned by cleaving

one edge of the flat surface, or in some cases a naturally occuring facet served just as well. The exciting nitrogen laser was focussed onto a variable width slit and an image of the slit was focussed onto the flat surface of the crystal with the length of the slit perpendicular to the edge and the image starting at the edge. Stimulated emission, unencumbered by spontaneous emission was observed from the edge. By varying the length of the slit the net gain in the cavity could be varied in such a way as to determine the gain spectrum.

The gain spectrum and its temperature dependence are best interpreted in terms of the electron-hole metallic droplet recombination mechanism, where the very ionic nature of GaN enhances the stability of this phase via the interactions of the electrons and holes with the very polar LO phonon. The large binding energy measured, 10 meV is in reasonable agreement with a simple model for the droplet including this interaction and results in a deduced low temperature liquid density of 4.4×10^{18} pairs per cm^3 and the phase diagram we construct from the data indicates the extremely high critical temperature of $81^{o}K$, the highest such temperature yet reported in any semiconductor.

By cleaving a second facet and focussing the nitrogen laser to completely fill the planar surface between the two edges, a normal optically pumped cavity is achieved and the spectra of the light emitted from either of the two edges as a function of pump density maps out the Fabry-Perot cavity modes at low pumping intensity and clearly indicates the onset of lasing in one or several of these modes as the power is increased.

Laser threshold measurements vs. cavity length indicate high over-all conversion efficiencies, quite comparable with good GaAs lasers at low temperatures and losses in this spectral range of only about 75 cm^{-1}. Again, when compared with the normal losses of typical GaAs lasers, about 30 cm^{-1},

it is obvious that our GaN crystals are really very good, relatively defect-free semiconductor crystals.

These results were obtained as a natural extension of the photoluminescence program described in the last section, but the reults do not help us very much towards achieving the main goals of this contract. Therefore, we will not belabor the description of these experiments, the results and their interpretation. However, we attach, as an Appendix to this Report, a complete account of this investigation for the interested reader.

APPENDIX

STIMULATED EMISSION, LASER ACTION AND ELECTRON-HOLE DROPLET RECOMBINATION

STIMULATED EMISSION AND LASER ACTION

It was reported that GaN has an external photoluminescence efficiency of about 5% at 78°K and 0.5% at room temperature[1]. We have found similar photoluminescence efficiencies at 4.2°K (or 77°K) and at room temperature. GaN has been shown to be a firect gap semiconductor with E_g = 3.500 eV at 2°K. Furthermore, the occurence of very high gain ($g = 10^5$ cm^{-1}) in the stimulated emission[2] indicates that GaN is a potential candidate as a laser material.

Stimulated emission and laser action have recently[2] been reported by Dingle et al. They determined the excited length and pump power dependence of the stimulated emission by gain measurements[3] at a temperature of 2°K only. They did not see any Fabry-Perot mode structure in the laser output and did not determine the cavity losses.

The present work represents the first detailed study of stimulated emission and laser action in gallium nitride at both LHe (4.2°K) and LN_2 (77°K) temperatures. In the first section the experimental arrangements for the optical gain measurements are described. These have enabled us to measure stimulated emission at various excitation lengths &

power densities. In the last section we describe the results, including optical gain, the dependences of excitation length and power density, threshold gain, cavity losses, Fabry-Perot mode structures, and the nature of laser transition as due to electron-hole droplet recombination.

A. Experimental Arrangements

We fabricated Fabry-Perot structures on epitaxial GaN and on whisker GaN crystals for the study of stimulated emission and laser action. Since epitaxial GaN is hard to cleave, most good Fabry-Perot structures were selected from whisker (needle-like) GaN crystals. The cavities had lengths of 400 - 1700 μm. Two cleaved R($1\bar{1}02$) plane surfaces defined the cavity length L, and the excitation was on a ($10\bar{1}0$) hexagonal face of the crystallites. Such a typical as-grown structure is shown in Scanning Electron Microscope and optical microscope photographs in Fig. 1.

After organic cleaning, the whisker GaN sample was mounted on a sample holder with silicone grease and immersed in the liquid helium dewar. All temperatures reported are sample temperatures. For the pump intensity used, sample heating is not expected to be significant.

(a) Optical Microscope picture ⊣300μ⊢

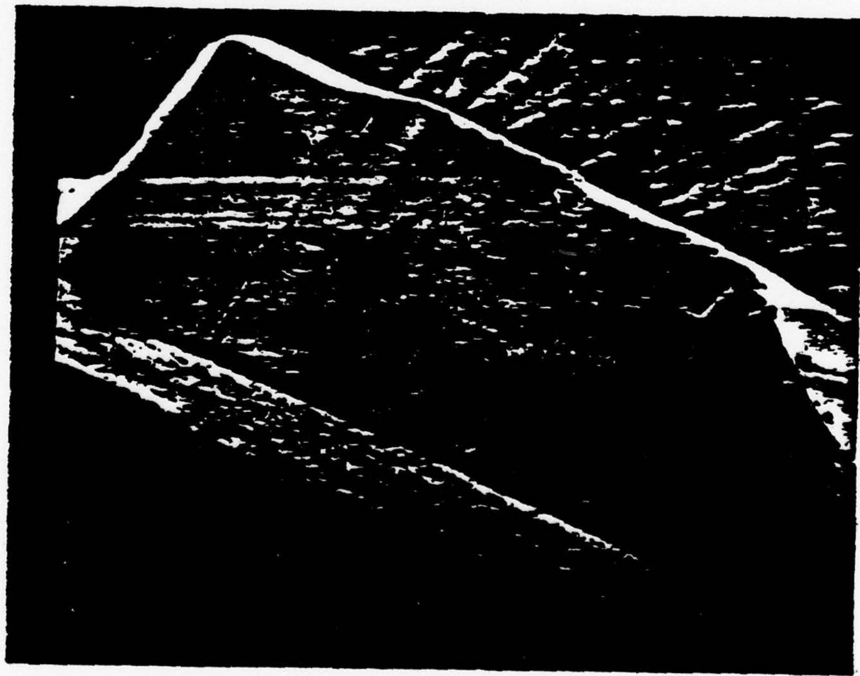

(b) Scanning Electron Microscope picture ⊣200μ⊢

Fig. 1 The shape of a typical cavity of whisker GaN

The experimental set up for gain measurements of the stimulated emission is shown in Fig. 2. The pump source was 3371 Å light from a pulsed (100 KW peak power, 10^{-8} sec duration time at repetition rate of 100 pps) N_2 laser. The cross-section of the laser beam is rectangular with typical dimensions of 5 x 0.2 cm and the intensity distribution along the long dimension is uniform to within 2%. The laser beam passed through a variable attenuator-neutral density filter (Oriel Optics Corp.) and was focused to a line by a cylindrical lens. An adjustable slit (Gaertner Scientific Corp.) placed at the focal plane of the cylindrical lens was used to control the length l of the exciting beam. The slit was imaged onto the sample by means of a spherical lens.

Typically the excited region had a width of less than 100 μm and a maximum length of about 2.0 mm. Under these conditions the maximum excitation intensity at the sample surface was 10 MW/cm^2. Considering the total losses of 50% (include 30% reflected by the GaN surface, 10% collective losses and 30% transmission losses in the quartz dewar walls, lenses and mirrors), the absolute maximum excitation intensity onto the GaN sample surface was about 5MW/cm^2.

The stimulated emission emerging from the edge of the sample, was focused on the entrance slit of Perkin-Elmer E-1 monochromator. The output signal of the spectrometer

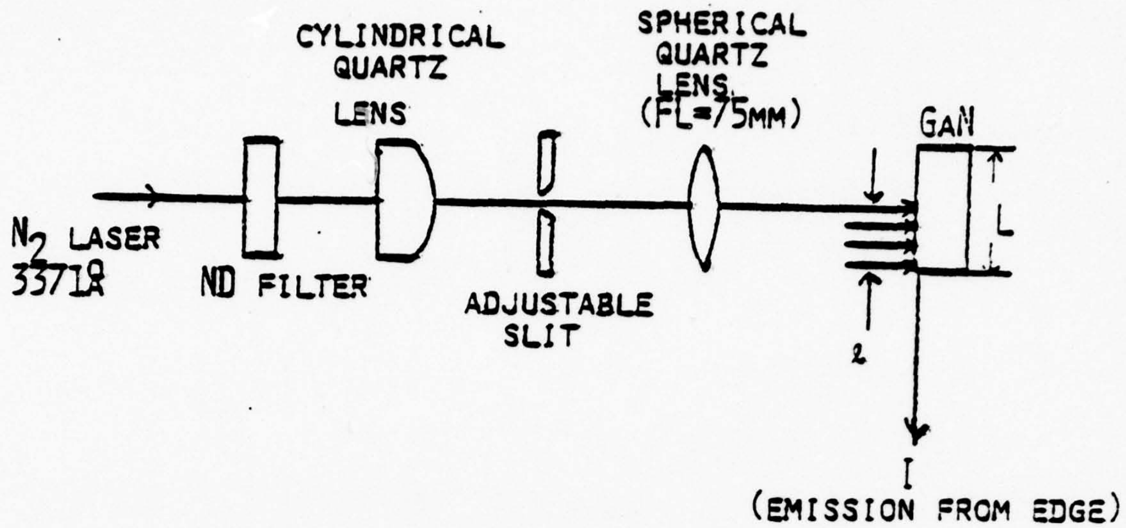

(A)

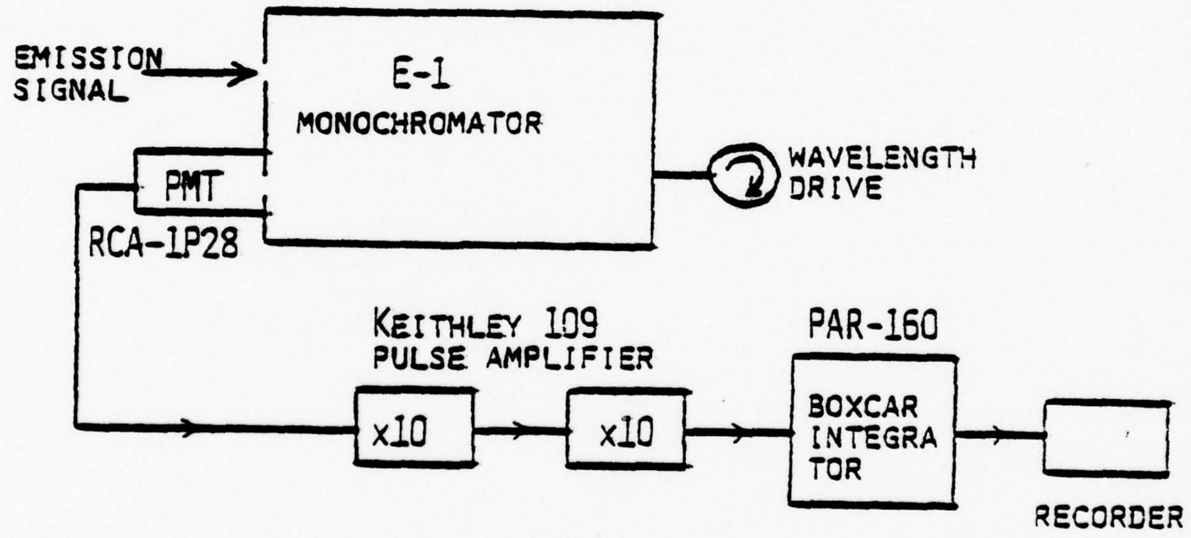

(B)

Fig. 2
(A) Optical and (B) electronic set up for the optical gain measurements

was detected by a fast photomultiplier (RCA-1P28) and averaged by a fast boxcar integrator (PAR model 160) with an aperture time of 20 nsec, a time constant of 300 nsec, and a time base of 2 μsec. The photomultiplier should have a risetime short compared to the pulse length of 10^{-8} sec, and should have a large maximum anode current for ease of subsequent electronic signal processing. The RCA-1P28 photomultiplier has the following characteristics: 9-stages, modified S-5 (104) response of 2000-6500 Å range, typical gain of 2.5×10^6, anode pulse rise-time of 2 nsec, average anode current of 0.5 mA and a dark current of 5 nA at an operating voltage of 1000 volts. Hence, this is a reasonably good photomultiplier for detecting nsec-pulsed signals. There are two pulse amplifiers (Keithley 109) between the PMT and the Boxcar to multiply the signal by a factor of 100. The output signal was recorded by a L & N chart recorder.

B. Results

We have observed stimulated emission in the 0.36 μm UV region from GaN whisker samples with optical pumping at liquid He temperature as shown in Fig. 3 . Similar results were obtained at liquid nitrogen temperature, as shown in Fig. 4 , with the lines shifted about 10 Å toward longer

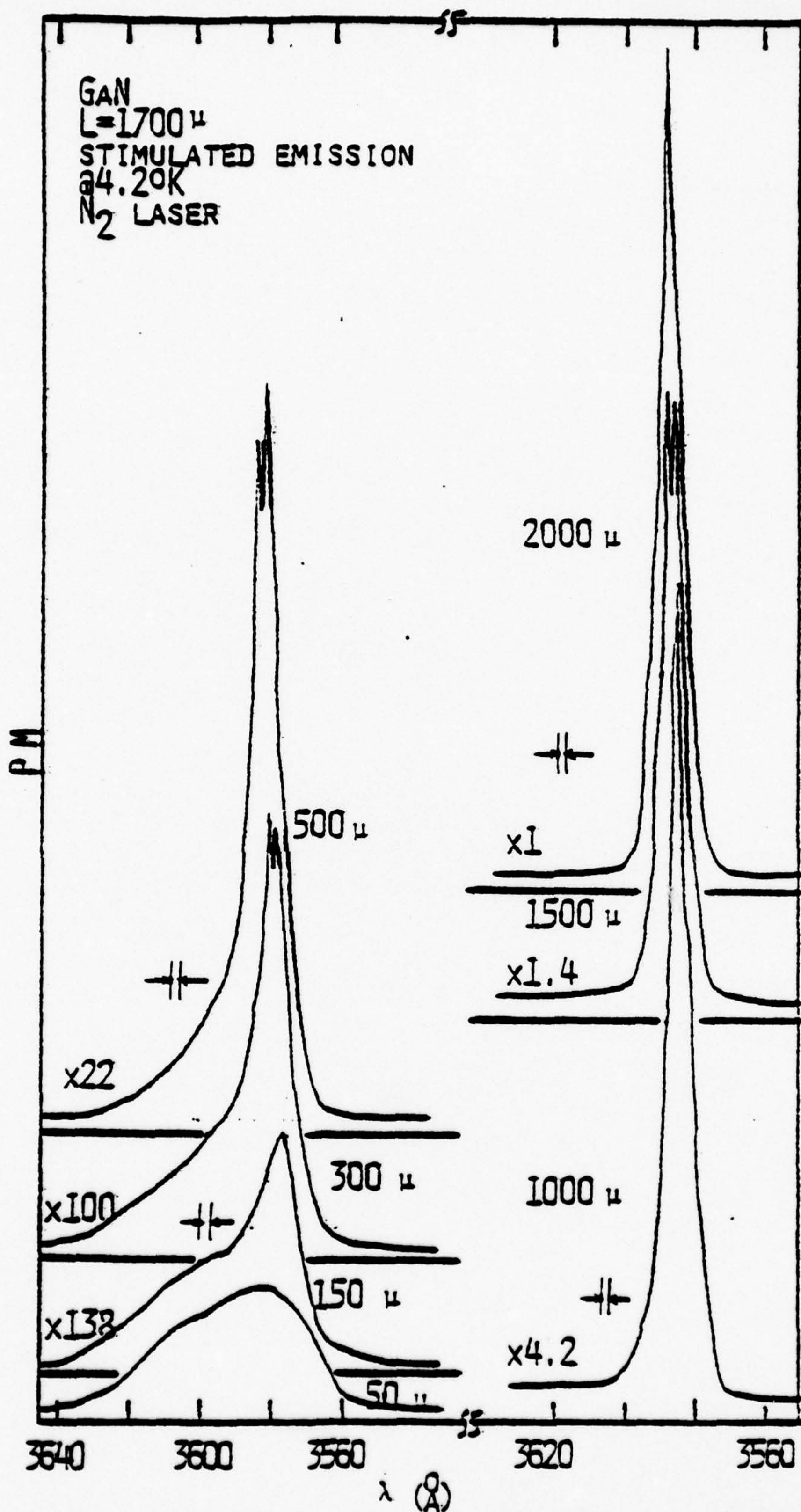

Fig. 5 The stimulated emission spectra as a function of excitation length at 4.2°K

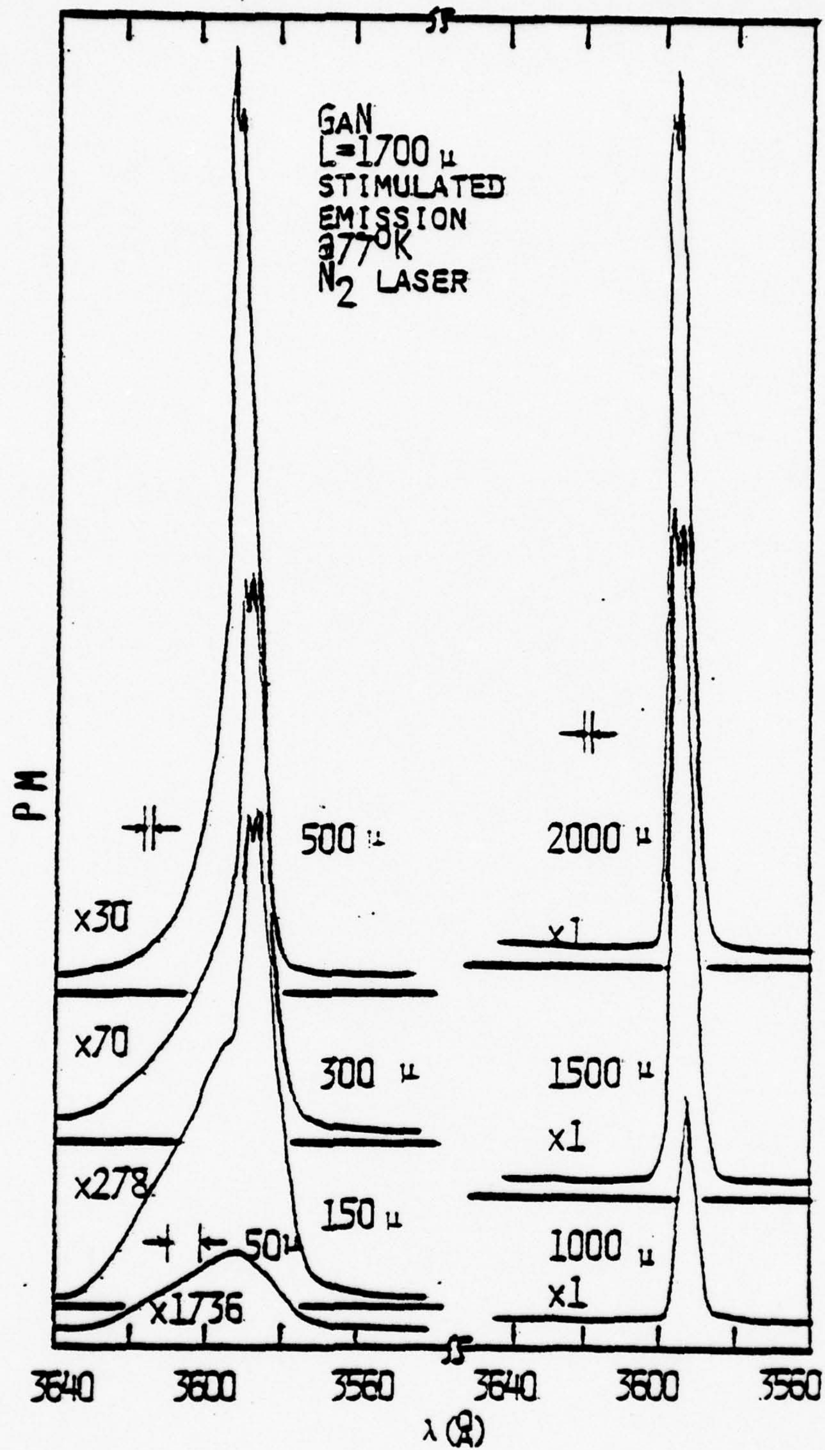

Fig. 4 THE STIMULATED EMISSION SPECTRA AS A FUNCTION OF EXCITATION LENGTH AT 77°K

wavelengths. The peak of the stimulated emission occurs at longer wavelengths than the spontaneous luminescence. The intensity of the stimulated emission increases more rapidly than linear (superlinear) with increases of either the excitation length or the excitation intensity.

The optical gain can be obtained from a plot of Ln I vs. ℓ. The threshold gain for lasing can be determined directly from the plot of I vs. P. Total cavity losses of about 70 cm^{-1} can be estimated from the reflection losses and internal losses as obtained from a plot of P_{th} against 1/L. Fabry-Perot mode structure has been observed with high spectral resolution. The nature of the laser transition as deduced to be by the electron-hole liquid (EHL) model is presented in the next section.

1. Excitation length dependence and optical gain

The stimulated emission spectra are shown in Figs. 3 and 4 as a function of excitation length at 4.2°K and 77°K, respectively. Stimulated emission can be identified as stimulated by the superlinear dependence of the output intensity at long wavelengths with increasing excitation length. Only the excitation length was varied to produce the observed shift of emission to longer wavelengths.

For shorter excitation lengths, there is a broad shoulder on the longer-wavelength side of the stimulated emission. This broad band emission which peaks at 3390 Å

and its relationship to lasing in GaN is discussed in the next chapter.

Over the region for which optical amplification dominates the output, I varies as $I(\ell) \propto \exp(g\ell)$ where g is the gain in cm^{-1} and ℓ is the excitation length. Using this relationship, the gain can be determined directly from the slope of the straight line portion (small ℓ region) of a curve of log I vs. length ℓ as shown in Fig. 5 . It indicates a net gain as high as 10^5 cm^{-1} at a wavelength of 3585 Å at the highest excitation power density of about 5 MW/cm^2 at 4.2°K. As the excitation length increases, log I increases linearly, followed by a region in which the exponential variation saturates.

The optical gain can be seen to vary from 3×10^4 to 10^5 cm^{-1} at 4.2 °K and from 4×10^3 to 5×10^4 cm^{-1} at 77°K.

2. Excitation density dependence and threshold gain

The near bandgap spontaneous emission at low excitation levels contains free exciton luminescence and various bound exciton lines in GaN. At high excitation levels (about 1 MW/cm^2) none of these emission lines were found to be important because they do not lead directly to stimulated emission. Instead, several new emission lines dominate the near bandgap spectra. They are located lower in energy than the bound exciton lines.

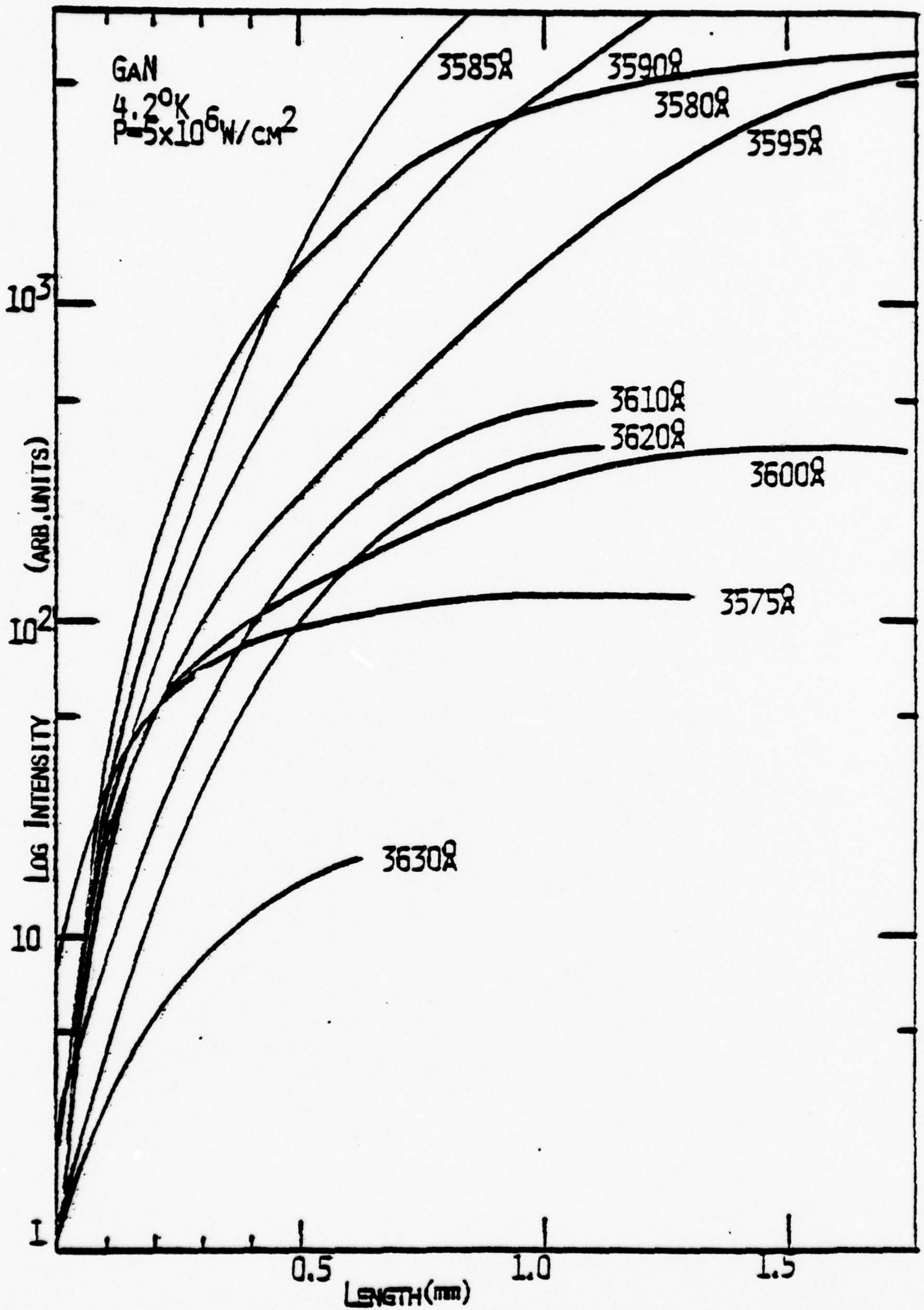

Fig. 5. Variation of intensity of the stimulated emission with the excitation length at various wavelengths

Detailed studies of the spontaneous and stimulated emission spectra have been made as a function of excitation level at temperatures of both 4.2°K and 77°K, as shown in Figs. 6, 7, and 8. At 4.2°K, the spontaneous emission spectra, corresponding to light emitted from the front surface of the crystal, exhibits a sharp line at 3572 Å which has already been identified as recombination of bound excitons. The peak position of the BE does not shift with increasing pump power density. A braod shoulder centered about 3595 Å is presumably due to electron-hole liquid recombination and is probably the origin of the laser transition. This is discussed in the next chapter.

Stimulated emission from the cleaved edges was measured at right angles to the pump beam and its peak occurs at longer wavelengths than the spontaneous emission. The peak of the stimulated emission shifts to longer wavelengths with increasing excitation power density as shown in Fig. 9. These two effects are characteristic of stimulated emission in a rather large class of undoped semiconductors such as CdS and GaAs.

The peak intensities of the spontaneous emission at 3572 Å and the stimulated emission at 3585 Å are shown in Fig. 10 as a function of excitation power density at 4.2°K. The excitation dependence for spontaneous emission ap-

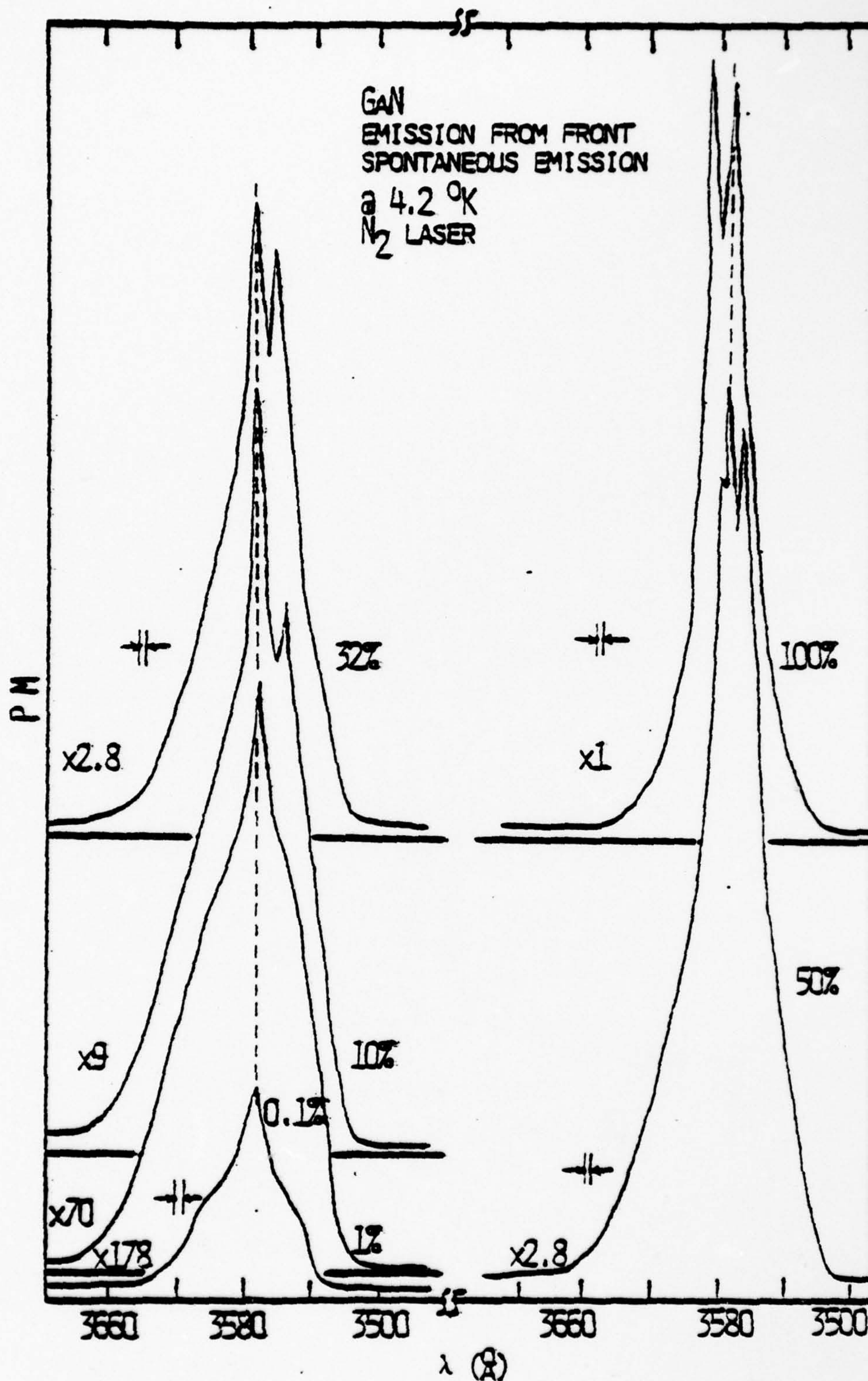

Fig. 6 THE SPONTANEOUS EMISSION SPECTRA AS A FUNCTION OF EXCITATION LEVEL AT 4.2°K

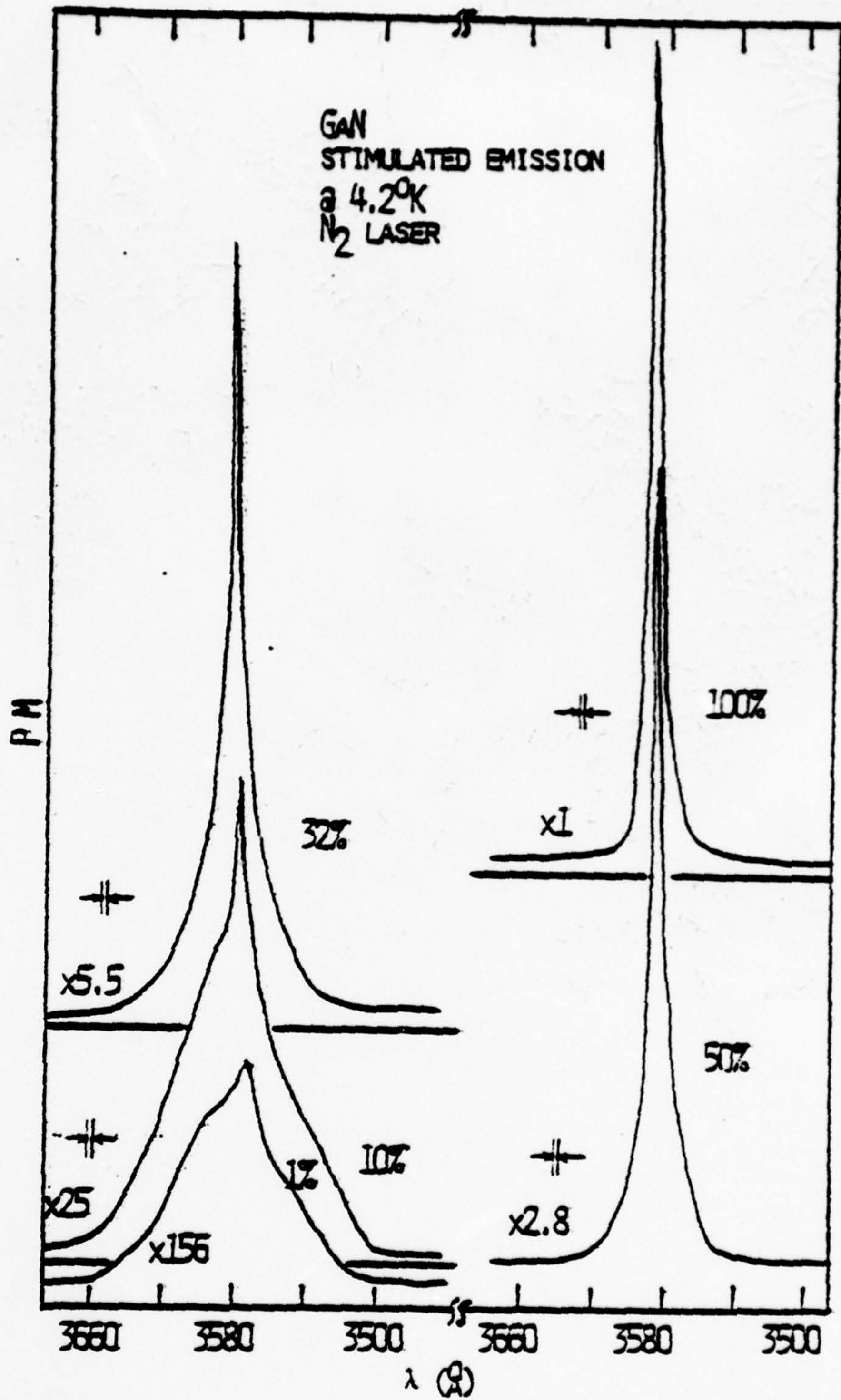

Fig. 7 THE STIMULATED EMISSION SPECTRA AS A FUNCTION OF EXCITATION LEVEL AT 4.2°K

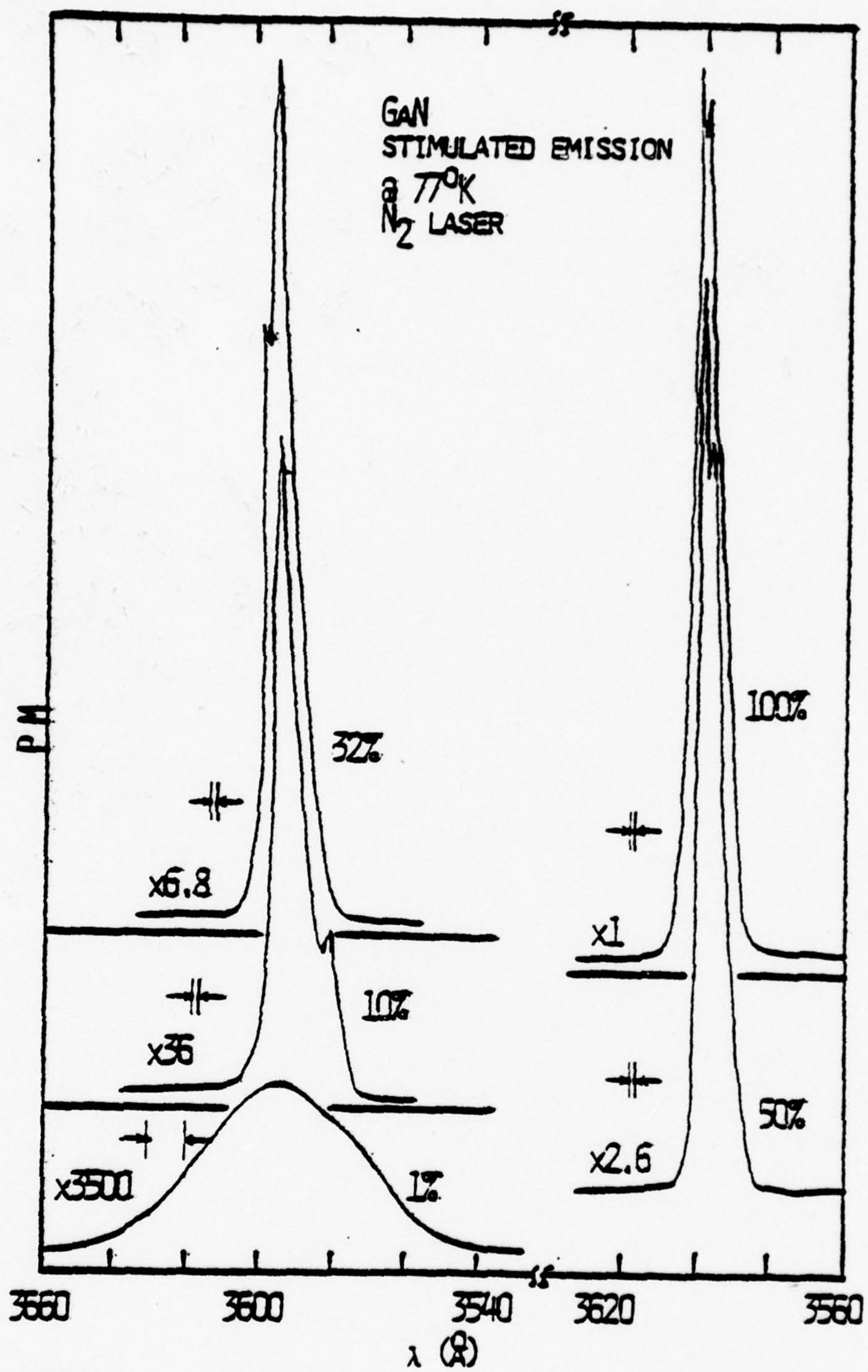

Fig. 8: THE STIMULATED EMISSION SPECTRA AS A FUNCTION OF EXCITATION LEVEL AT 77°K

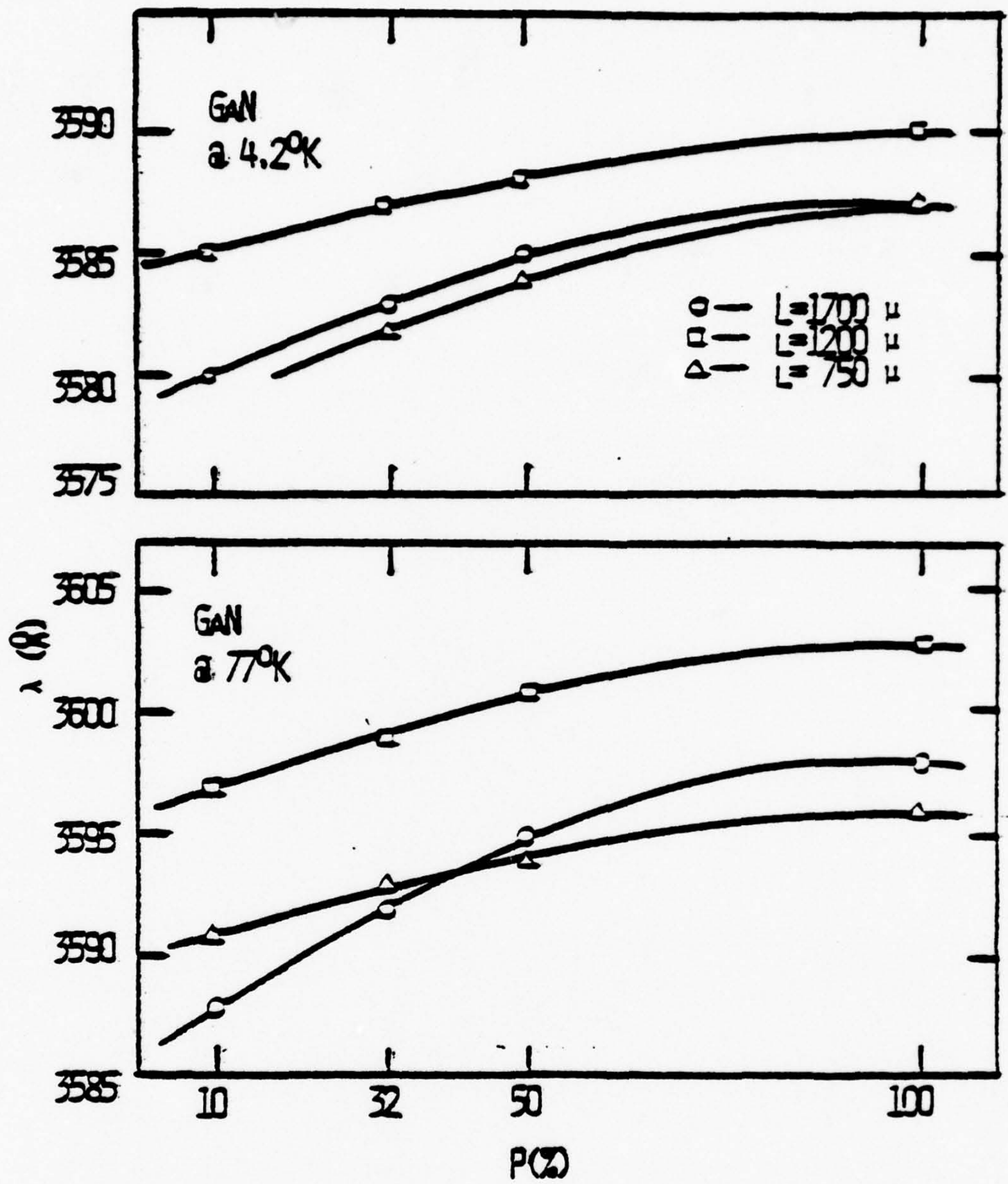

Fig. 9 THE PEAK OF STIMULATED EMISSION SHIFTS TO LONGER WAVELENGTHS WITH INCREASING EXCITATION POWER DENSITY

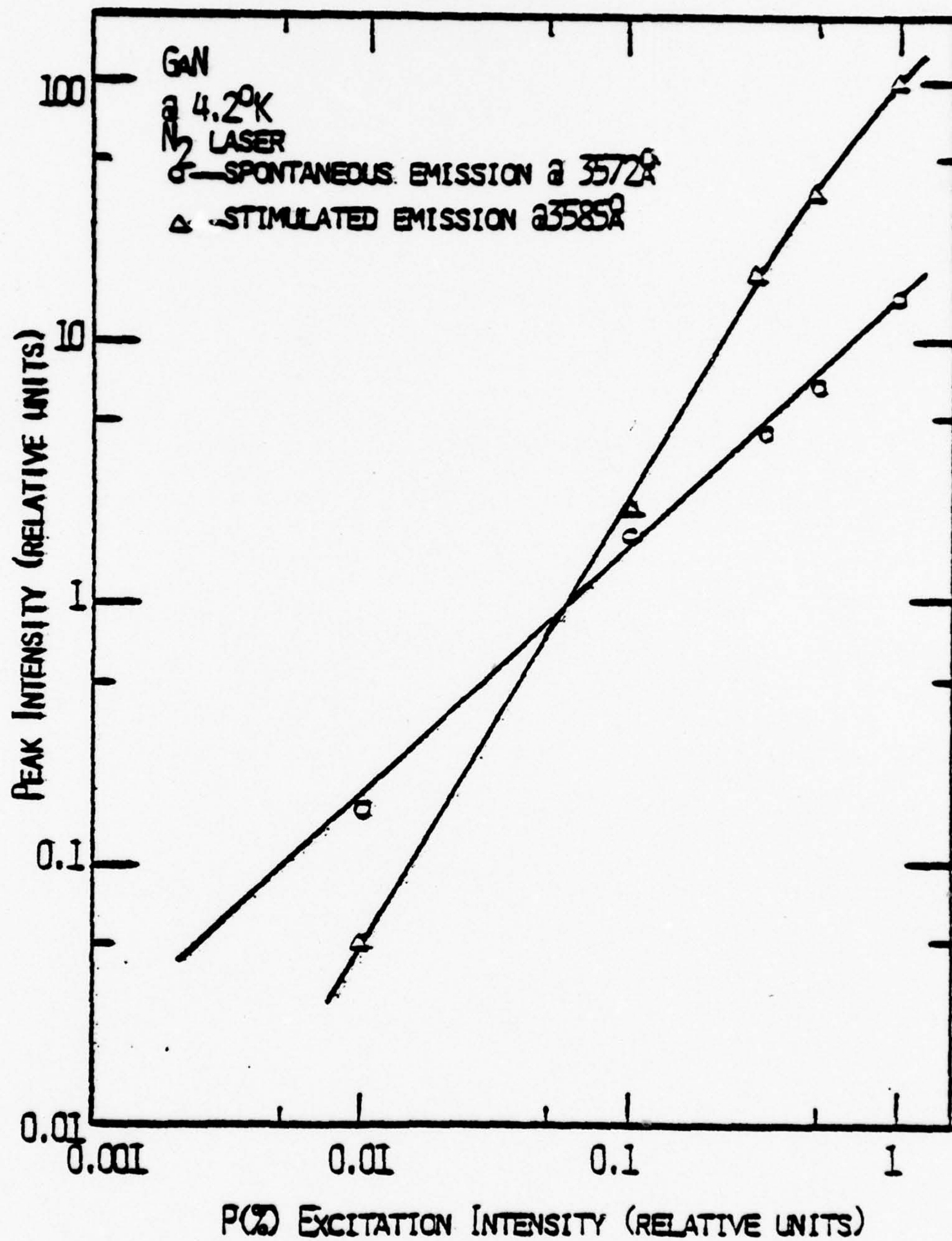

Fig. 10 THE PEAK INTENSITIES OF THE SPOTANEOUS EMISSION AT 3572Å AND THE STIMULATED EMISSION AT 3585Å AS A FUNCTION OF EXCITATION POWER DENSITY AT 4.2°K

proaches a linear dependence. The intensity of the stimulated emission increases more rapidly than linear (superlinear) with increasing excitation intensity. This superlinear dependence establishes the existence of stimulated emission.

The peak half-widths (FWHM) of the spontaneous and stimulated emissions are shown in Fig. 11 as a function of excitation power density at $4.2^{o}K$. The spontaneous emission band exhibits a half-width of about 40 - 50 Å over the entire range of pump power density described here. The half-width of the stimulated emission peak decreases abruptly from about 40 Å at low excitation intensity to about 7 Å at high excitation intensity at the threshold pumping power for laser oscillation. Furthermore, at low pumping power there is spontaneous emission emitted in all directions, whereas at the higher powers the emission is stimulated emission.

From the plot of I vs. P we can determine directly the threshold pumping power density for lasing. The excitation dependence for different cavity lengths, L = 400-1700 μm, at both $4.2^{o}K$ and $77^{o}K$ are shown in Fig. 12 and 13, respectively. The threshold pumping power densities are 1.55, 1.10, 0.85 and 0.75 MW/cm^2 at $4.2^{o}K$ and 1.65, 1.10, 0.90 and 0.80 MW/cm^2 at $77^{o}K$, corresponding to cavity lengths 400, 750, 1200, and 1700 μm, respectively.

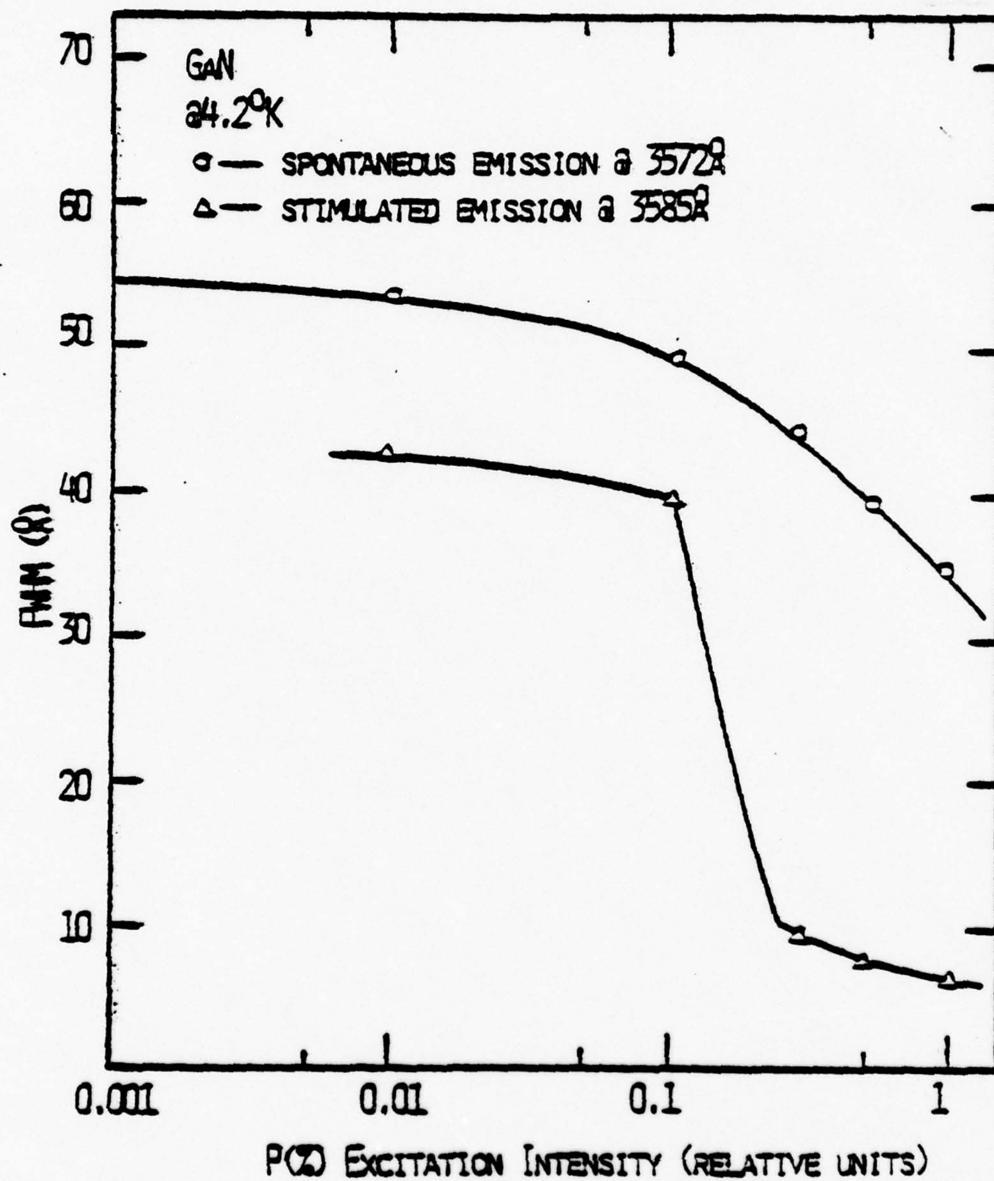

Fig. 11 THE PEAK HALF-WIDTH (FWHM) OF SPONTANEOUS AND STIMULATED EMISSION AS A FUNCTION OF EXCITATION POWER DENSITY AT 4.2°K

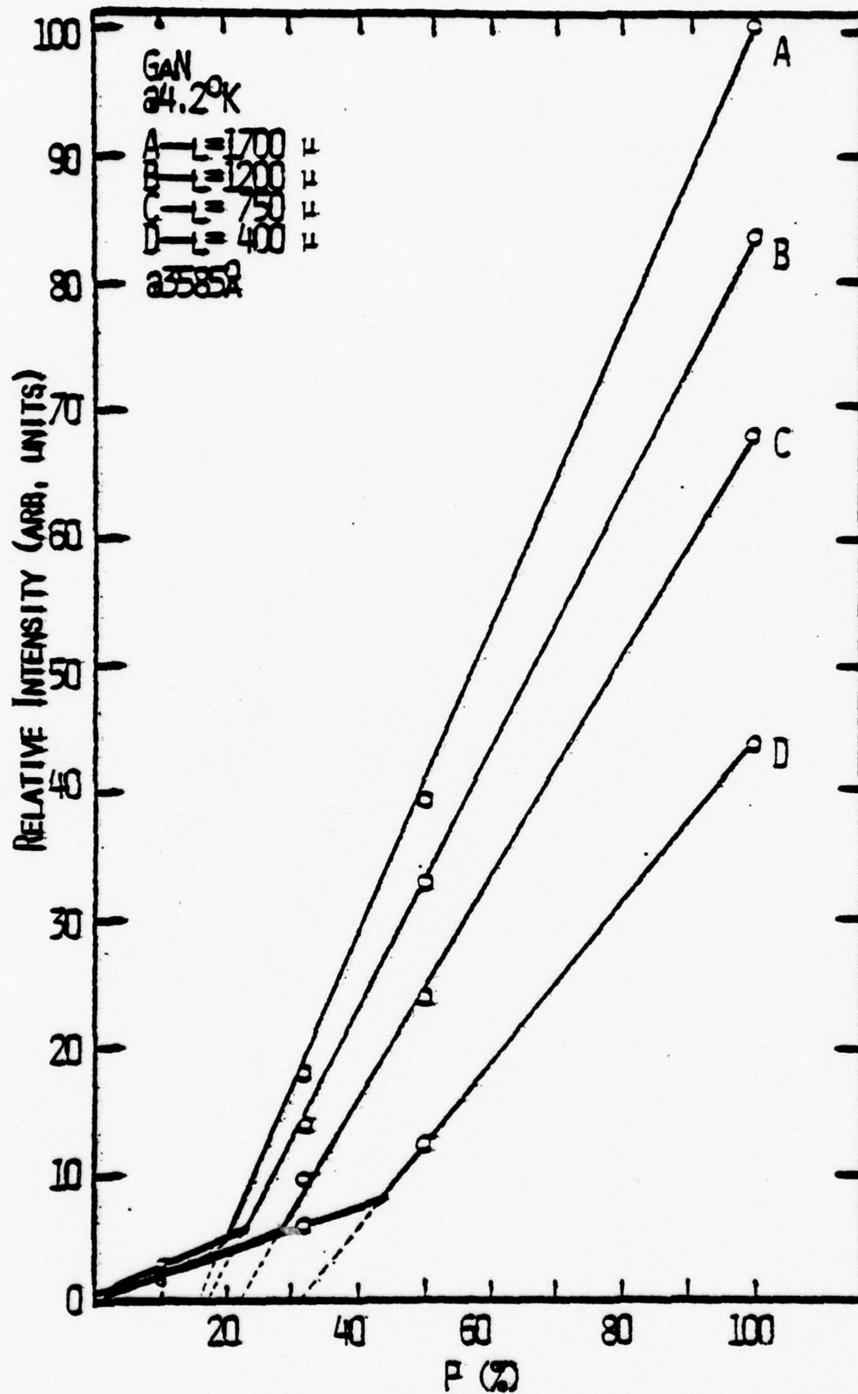

Fig. 12 THE EXCITATION DEPENDENCE OF DIFFERENT CAVITY LENGTH L AT 4.2°K

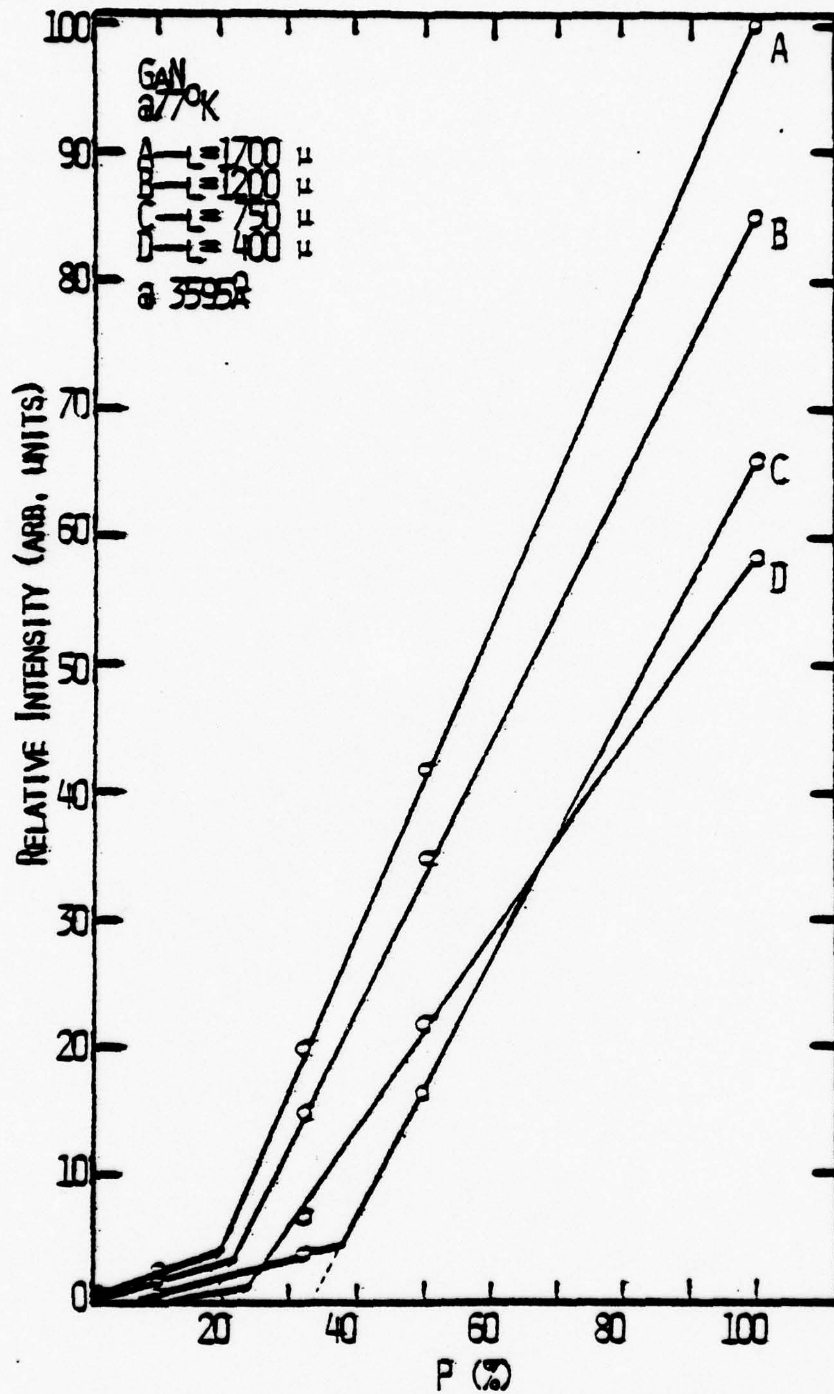

Fig. 13 THE EXCITATION DEPENDENCE OF DIFFERENT CAVITY LENGTH L AT 77°K

3. Cavity losses

For a resonant Fabry-Perot cavity, the threshold condition for laser oscillations is very simple. It contains the optical gain g (cm^{-1}), the internal laser losses (free carrier absorption, penetration losses, diffraction and defect-center scattering losses), and the reflection losses due to the reflectivity coefficient R at the laser ends.

At threshold, the total gain in the structure must equal the sum of total internal and end losses, i.e., $\alpha_T = \alpha_R + \alpha_I$. The threshold condition for the laser cavity is given by:

$$e^{(g-\alpha_T)L} = 1 \quad (10)$$

$$e^{-\alpha_R L} e^{(g-\alpha_I)L} = 1$$

$$g_{th} = \alpha_I + 1/L \, Ln 1/R = \beta P_{th} \quad (11)$$

Finally, the threshold pumping power density equation is given by:

$$Pth = \alpha_I/\beta + 1/L \, (1/\beta \, Ln \, 1/R) \quad (12)$$

where g_{th} = threshold gain

P_{th} = threshold for pumping power density

β = gain factor

α_I = internal laser losses

L = cavity length

R = reflectivity of the ends of the cavity

We have studied the dependence of P_{th} on laser cavity length, L, as shown in Table 1 . Equation (12) predicts a linear dependence. Figure 14 shows experimental results at both $4.2^{o}K$ and $77^{o}K$ for a set of GaN whisker laser cavities with different cavity lengths (400 μm to 1700 μm).

As can be seen, the linear relation holds very well at both $4.2^{o}K$ and $77^{o}K$. With short pulses of 10 ns duration and a repetition rate of 80-100 pps, sample heating could be neglected even at the highest power densities. This dependence indicates that the gain is linearly dependent on the excitation power density both at $4.2^{o}K$ and at $77^{o}K$.

The reflectivity of GaN at 3.45 eV in energy is about 15%[4]. Thus we can estimate reflection losses to be about 50 cm^{-1}. We note from Fig. 14 that, for a given cavity length, e.g., 4×10^{-2} cm, the threshold power density increases slightly from 1.55 MW/cm^2 at $4.2^{o}K$ to about 1.65 MW/cm^2 at $77^{o}K$. The corresponding gain factor β decreases from 47.43 cm/MW to 44.64 cm/MW, and the internal loss factor α_I increases from 24.14 cm^{-1} to 25.89 cm^{-1}. It is clear that the threshold pumping power densities for laser action and the total cavity losses are almost the same both at $4.2^{o}K$ and at $77^{o}K$. P_{th} should increase at temperatures greater than $77^{o}K$.

TABLE 1

DEPENDENCE OF THE THRESHOLD PUMPING POWER DENSITY P_{th} FOR LASER ACTION ON THE CAVITY LENGTH L

(1) at 4.2°K

L (μm)	1/L (cm^{-1})	P_{th} (%)	P_{th} (MW/cm^2)
1700	5.9	15	0.75
1200	8.33	17	0.85
750	14.3	22	1.10
400	25.0	31	1.55

(2) at 77°K

L (μm)	1/L (cm^{-1})	P_{th} (%)	P_{th} (MW/cm^2)
1700	5.9	16	0.80
1200	8.33	18	0.90
750	14.3	22	1.10
400	25.0	33	1.65

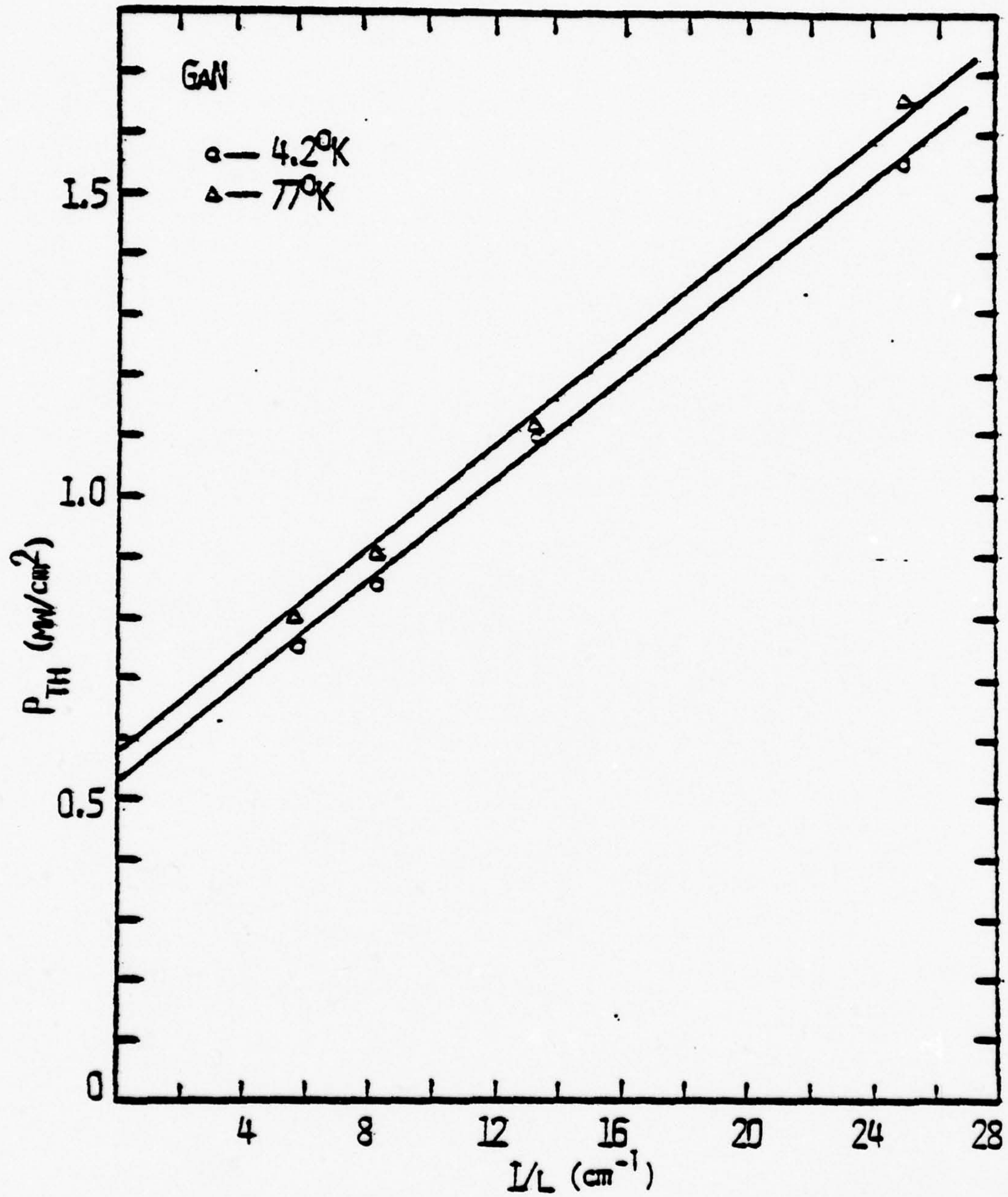

Fig. 14 EXPERIMENTAL RESULTS OF THE DEPENDENCE OF THE THRESHOLD POWER DENSITY P_{TH} ON THE CAVITY LENGTH L AT BOTH 4.2°K AND 77°K

4. Fabry-Perot mode structure

a. Calculation of mode separation

A standing wave is produced in a Fabry-Perot cavity only if its length L contains an integral number of half-wavelengths, the wavelength measured inside the medium. Thus, $nL = m(\lambda/2)$, where λ is the wavelength in vacuum, n is the index of refraction of the medium, and m is the integral order number. For $m > 1$ the wavelength separation between two modes is then $\lambda^2/2L(n - \lambda(dn/d\lambda))$, where in general n is a function of wavelength. For the lasing wavelength 3595 Å, L = 400 µm, and n = 2 (assuming it to be independent of wavelength), we can estimate a mode spacing of about 0.8 Å

b. Experimental results:

With high spectral resolution (0.28 Å), the laser lines do indeed exhibit the familiar Fabry-Perot cavity mode structure, typical examples of which are shown in Figs. 15 and 16. We found that it consists of fourteen equally spaced modes (mode #3 and #13 are missing for some unexplained reason) whose separation is about 0.8 - 0.9 Å, in agreement with the calculated value of mode spacing. The peak positions of the lasing modes are shown in Fig. 17 as a linear function

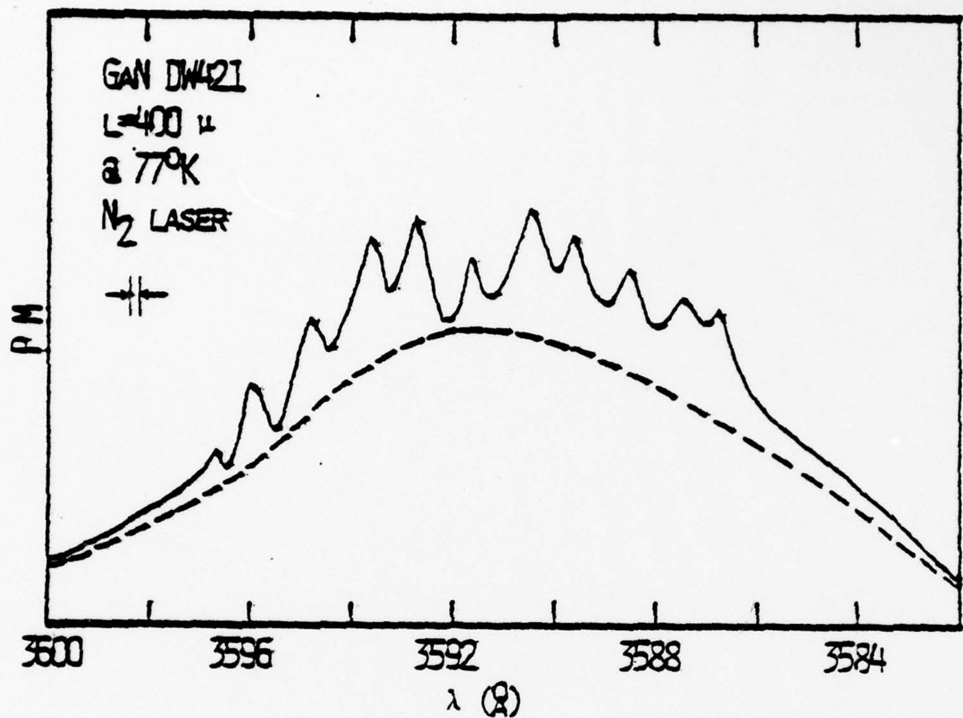

Fig. 15 EXPERIMENTAL HIGH-RESOLUTION SPECTRAL DISTRIBUTION OF THE FABRY-PEROT MODE STRUCTURE

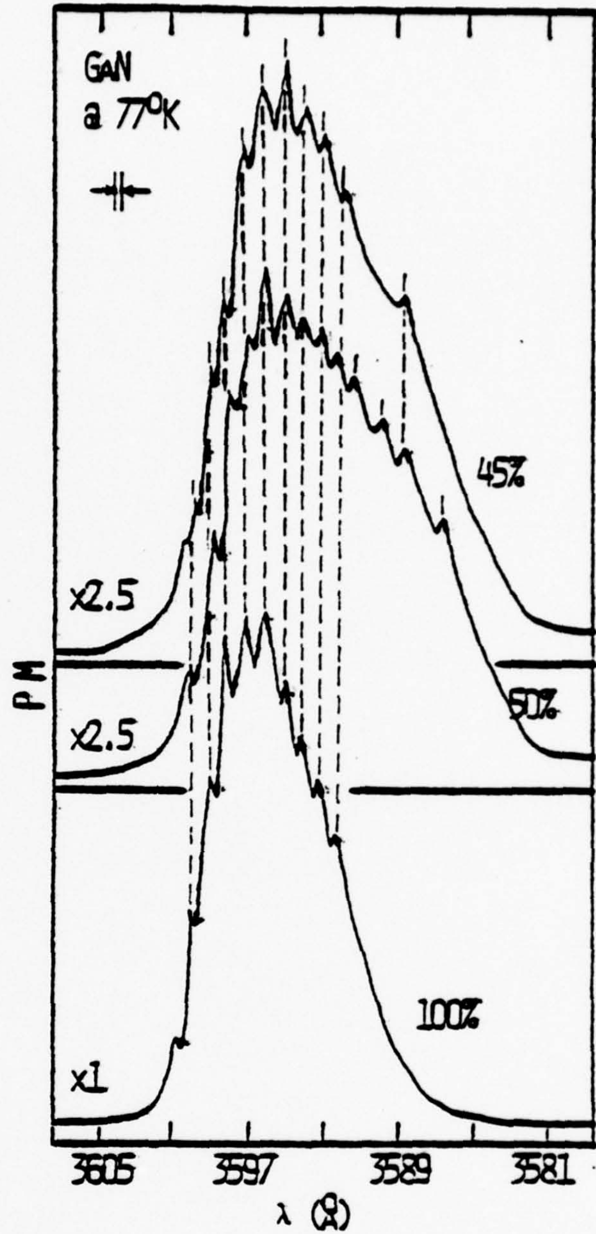

Fig. 16 EXPERIMENTAL HIGH-RESOLUTION SPECTRAL DISTRIBUTION OF THE FABRY-PEROT MODE STRUCTURE WITH DIFFERENT EXCITATION POWER DENSITY

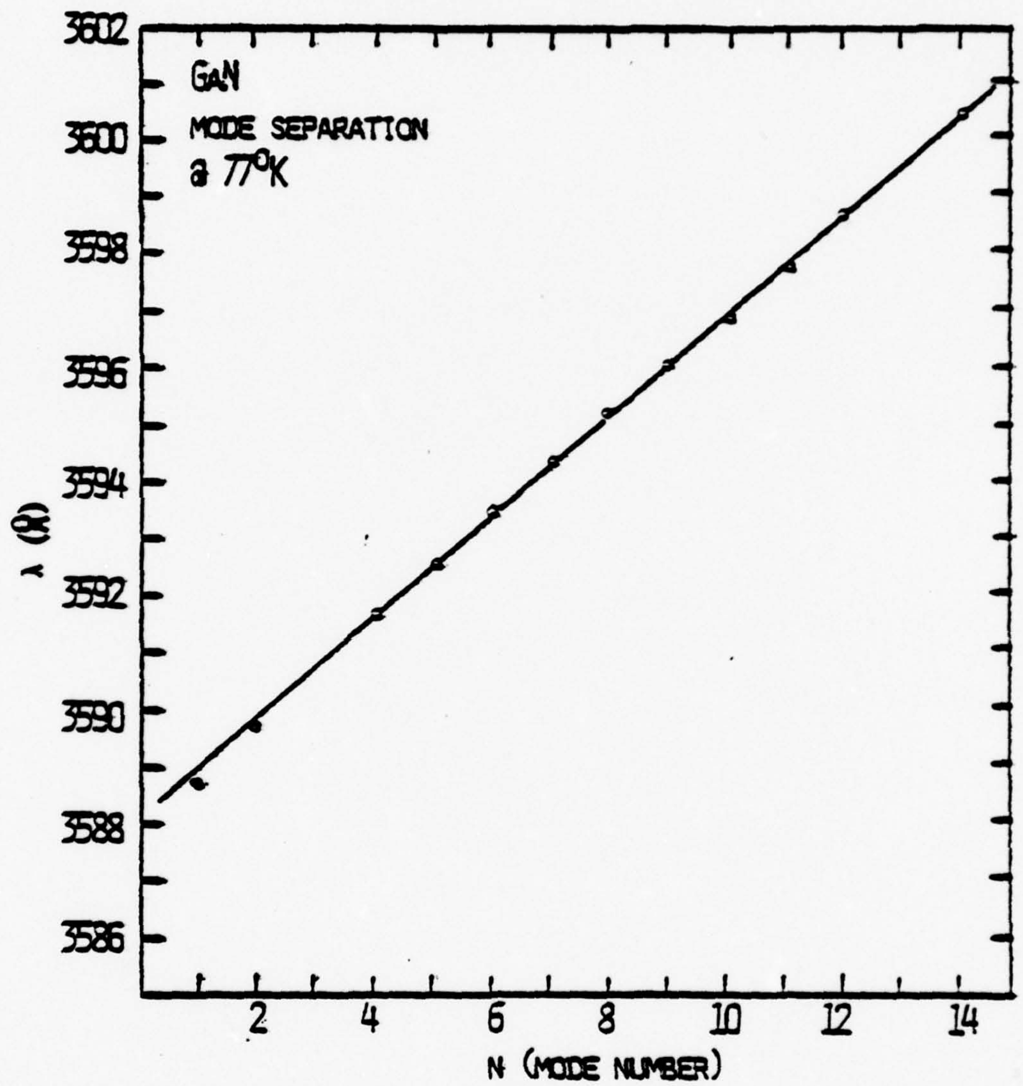

Fig. 17 THE PEAK POSITIONS OF THE LASING MODES AS A LINEAR FUNCTION OF THE MODE NUMBER

of the mode number. Because the cavity is not a simple Fabry-Perot structure, there are cavity length L variations with different excitation penetration depths. This effect could give rise to the broadened mode structure we observed.

ELECTRON-HOLE LIQUID RECOMBINATION

A. Gain Spectra And Nature Of The Laser Transition

In this chapter, we will try to understand the nature of the lasing transition in GaN. We have described the gain measurements on GaN whisker samples in the previous chapter. The origin of the stimulated emission is due to the broad emission band which extends up to about 65 meV below the free-exciton line (E_{gx}) at 4.2°K and the lower used excitation levels. These optical gain measurements show that the emission spectra alone are not sufficient to analyze the optical transitions involved at high excitation levels. It was found that the optical gain in GaN with its particular wavelength and intensity dependence can distort the spectra of the emission peaks considerably. Therefore, physical conclusions as to the transition processes involved should be based on the spectral gain profile.

The gain spectra of the stimulated emission peak was obtained by analyzing the luminescence intensity vs. excitation length data as first described by Shaklee and Leheny[3]. The complete gain spectra for GaN at both 4.2°K and 77°K are presented in Fig. 18 as a function of wavelength below the band gap.

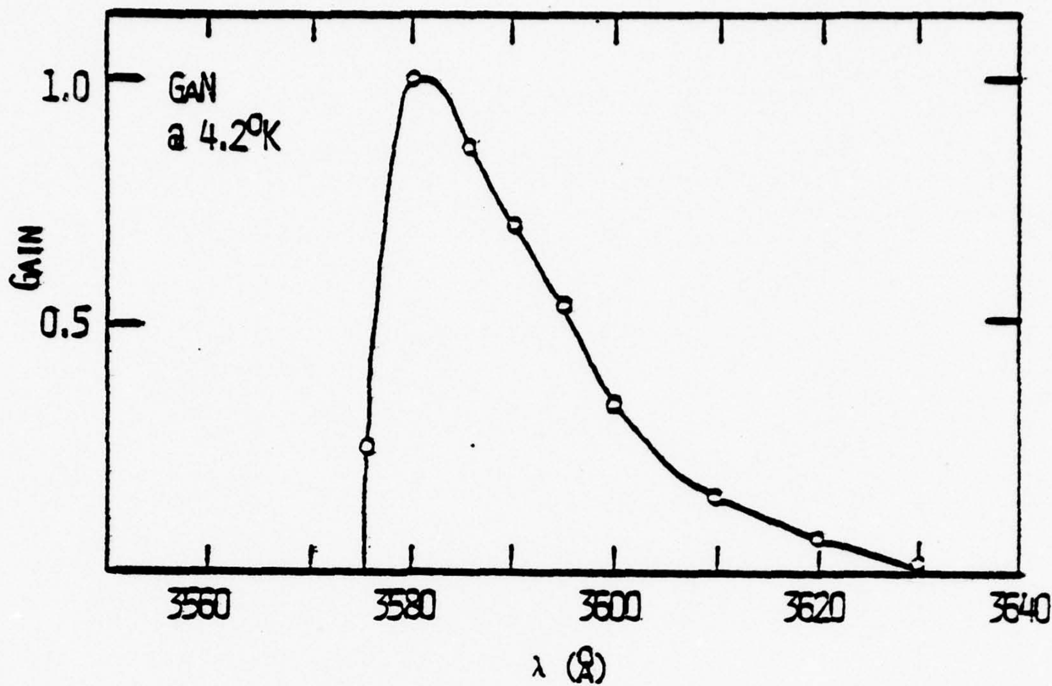

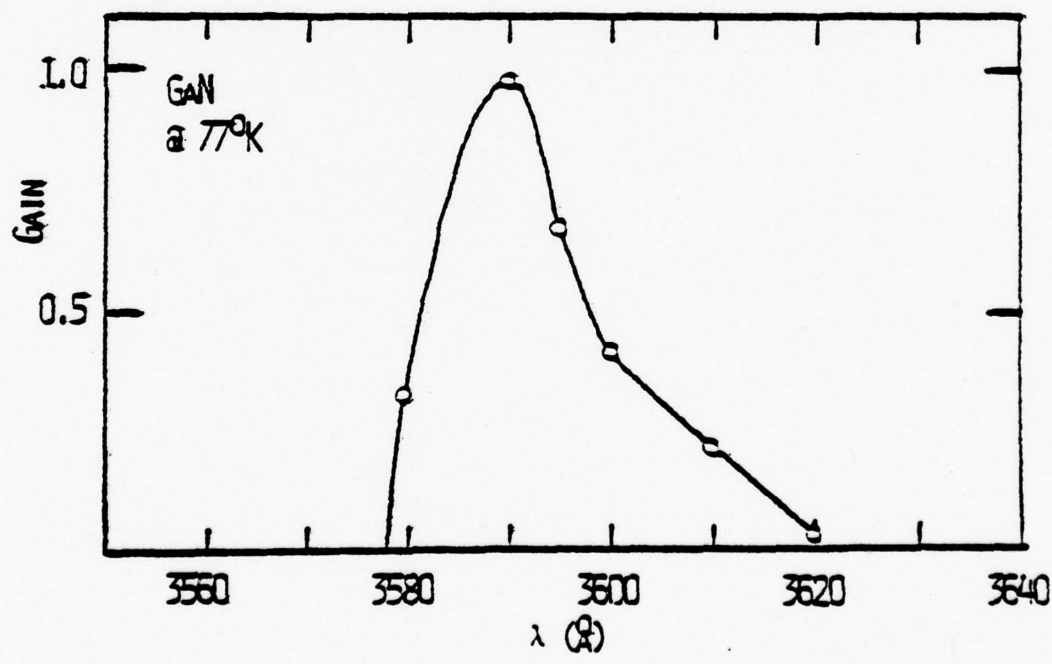

Fig.18 GAIN SPECTRA OF GaN AT BOTH 4.2°K AND 77°K, THE PUMP POWER DENSITY IS 5 MW/cm^2.

The gain distribution is asymmetric with a long wavelength tail. Over the range of pump power density investigated (0.5 - 5.0 MW/cm^2), there is no measurable gain at or above the bandgap for either temperature. In addition, the peak of the gain spectra does not shift appreciably when the excitation intensity is varied by a factor of 10. The gain linewidth, measured from the high-energy edge to the low-energy edge of the gain spectra, is also independent of the pump power density at $4.2^{o}K$. From the above experimental results, we have strong evidence to presume that the electron-hole liquid (EHL) exists in this polar semiconductor, GaN. This origin of the laser transition, based on recombination in a degenerate electron-hole liquid is a more reasonable explanation than one based on an exciton-exciton interaction process(5).

B. Review of Electron-Hole Liquid

1. EHL in indirect gap semiconductors

The phenomenon of EHL formation in highly excited indirect semiconductors like Ge and Si is now well understood both experimentally and theoretically(6).

It is known that non-equilibrium electrons and holes in semiconductors are bound in excitons at low temperatures by the Coulomb attraction between them. In fact,

almost all the electrons and holes are bound into excitons within a few mW/cm^2. At high exciton concentrations obtained by increasing the intensity of the exciting light, the interactions between them leads to the formation of a collective phase of electrons and holes.

In 1968 Keldysh first suggested that free excitons (FE) of sufficient densities could condense into a degenerate electron-hole plasma, which is electrically conducting, in order to explain anomalous photoconductivity observed in Ge. Although the analogy is not exact, the phenomenon of EHL is roughly analogous to the condensation of waver vapor into fog droplets.

Exciting light incident on a pure crystal is absorbed near the surface, generating free electrons and holes; these quickly form excitons, which diffuse up to a millimeter or so away from the surface. A droplet embryo may be formed from a statistical fluctuation in the exciton density in a pure crystal. If the radius of the droplet embryo is larger than the critical radius (~0.05 μm), it can grow to observable macroscopic metallic liquid drops containing equal numbers of electrons and holes.

Both the FE and the EHL will decay due to the anhilation of electron-hole pairs. The photoluminescence spectrum of FE and EHL in Ge (or Si) at an optical excitation

just above threshold for the formation of the drop phase, shows the broad line shape characteristic of the metallic drops. Detailed analysis yields the Fermi energy E_F and the condensation energy ψ.

The stability of the EHL is strikingly dependent on band structure. In Ge and Si, the complication in the band structure turns out to be favorable for condensation. And this is why the luminescence due to EHL was originally observed only in Ge and Si. The four equivalent valleys of Ge and six valleys of Si in the conduction band effectively reduce the electron Fermi energy by a factor of $(4)^{-2/3}$ and $(6)^{-2/3}$, respectively. The multivalley structure and mass anisotropy of Ge and Si together with their indirect bandgap, are responsible for the observed stability of EHL in these crystals. Both Ge and Si are indirect bandgap semiconductors, that is, electron-hole radiative recombination must be accompanied by the generation of a lattice vibration, a phonon. This reduces the transition probability and gives longer exciton lifetimes, which is favorable for drop formation.

2. EHL in polar semiconductors

For direct band gap semiconductors like GaAs and CdS the calculation of the EHL binding energies by Brinkman and Rice[7] was not encouraging. Because the small electron effective mass and the single conduction band minimum were unfavorable for EHL binding.

In the case of GaAs, the conduction band has a simple, spherical, parabolic band shape, and the electron effective mass is very small ($\approx 0.07\ m_0$). So it can not reduce the kinetic energy sufficiently, and the condensation of the non-equilibrium carriers in this semiconductor does not lead to an energy lowering at any concentration of excitons, i.e. the binding energy per electron-hole pair in the plasma is close to that of the free exciton. In addition, GaAs has a direct band gap with no phonon assistance during recombination. Hence it does not have a long enough exciton lifetime to form a drop. So it is hard to observe EHL in GaAs, CdS etc.

Recently, it has been shown theoretically by G. Beni and T. M. Rice[8] that the electron-phonon interaction plays an important role in the stabilization of the EHL phase in polar semiconductors. They have calculated the ground-state energy of the EHL including coupling to LO phonon, and found that the polar coupling increases the stability of the liquid phase relative to excitons. They have also applied the theory to AgBr and to direct bandgap semiconductors like CdS, CdSe and ZnS; and found that the EHL is strongly bound in CdS and AgBr but only weakly so in CdSe.

A similar conclusion has been reached by Keldysh and Silin[9]. Recently, M. Rösler and R. Zimmermann[10] have reported phase diagram calculations of EHL in excited direct gap semiconductors. Results were given for CdS, CdSe, ZnS, GaAs and CdTe.

Experimental identifications of the EHL phase in such highly excited polar semiconductors as CdS[11-14], CdSe[11], GaAs[15] and AgBr[16] have been reported recently and these measurements are in good agreement with the calculations of Beni & Rice and Rosler & Zimmermann as shown in Table 2.

The dominant effect of both electron-electron and electron-phonon interaction is to add a self-energy shift to the bare band energies. Usually, the self-energy is screened by the coulomb interaction. In polar crystals screening is due to lattice vibrations as well as to the electronic excitation. The self-energy shift which is the sum of exchange and correlation energies has only a weak k-dependence and does not change much with temperature[7]. Therefore, the shifted energy-gap can be calculated by taking the lowest-order diagram with the interaction screened by the dielectric function only at zero temperature and at the Fermi-momentum related to the density via $n = k_F^3/3\pi^2$.

TABLE 2

Theoretical and experimental results of EHL

	Theory*							Experiment		
	E_x (meV)	Δ^{LO} (meV)	n_o (cm^{-3})	$E_{o,min}$ (meV)	ϕ (meV)	n_c (cm^{-3})	T_c (^oK)	n_o (cm^{-3})	ϕ (meV)	T_c (^oK)
CdS	27	-79	2.6×10^{18} 5.5×10^{18}	-121	13 14	7.8×10^{17}	64	2×10^{18} 1×10^{18}	13 12	55
CdSe	15	-39	4.0×10^{17} 8.3×10^{17}	-59	0 5	1.2×10^{17}	30	4×10^{17}	2	
ZnS	36	-79	4.2×10^{18} 8.3×10^{17}	-127	7 12	1.4×10^{18}	79			
AgBr	16		6.2×10^{18}		14			8×10^{18}	55	70
GaAs	3.5	-10.4	3.4×10^{16}	-15.7	1.8	4.3×10^{16}	6.5	3×10^{16}	4.7	
CdTe	11	-24.5	2.9×10^{17}	-36.4	0.9	4.4×10^{16}	18			
SiC	20							7.8×10^{18}	19.5	41
GaN	30					1.3×10^{18}		4.4×10^{18}	10	81

* Parameters required: m_c, $m_{v,//}$, $m_{v,\perp}$, ε_o, ε_∞, $\hbar\omega_L$.

The self-energy shift due to an anisotropic energy band with longitudinal and transverse effective masses comes out to be the polaron shift Δ^{LO} without excitation. The EHL energies should be related to the exciton energy:

$$E_{ex} = E_g + \Delta^{LO} - E_x \tag{13}$$

Finally, the binding energy of EHL with respect to the exciton gas is given by

$$\psi = \Delta^{LO} - E_x - E_{o,\,min.} \tag{14}$$

where $E_{o,\,min.}$ the minimum of the ground-state energy of EHL is measured from a plot of E_o vs. n.

The standard way to investigate the EHL in highly excited semiconductors is to measure the luminescence spectrum. The EHL peak shows up as a broad band with increasing excitation. For the direct band gap semiconductors, gain measurements have proved to be a very powerful tool for investigating EHL[17] because the EHL creates a population inversion resulting in large optical gain. The normal recombination luminescence spectra will be distorted due to the wavelength dependent amplification of luminescence. Therefore, luminescence studies are unreliable for determining EHL properties. However, the gain spectra can be used directly to establish the distribution of excited states in the direct gap crystals.

Since the absorption changes sign at $h\nu = \mu(n,T)$ for all temperatures, the position of the chemical potential can be determined. When this cross-over point remains fixed in energy over a large region of excitation intensity there is strong evidence that EHL with an equilibrium density $n(t)$ is formed. At zero temperature, $\mu(n,T)$ for the equilibrium density n_o, μ_o, coincides with the minimum of the EHL ground-state energy $E_{o,\ min.}$, and this is the way the experimental value for the binding energy of EHL ψ is deduced.

$$\psi = E_{gx} - \mu(n_o,\ 0^oK) = A(FE) - \mu_o \qquad (15)$$

The line-width of the gain spectrum is usually taken as the Fermi energy E_F, and the excited carrier density n is calculated from this value for given temperature and the known band masses. Determination of the binding energy of EHL and the Fermi energy from the theoretical prediction and from the experimental gain spectrum are shown in Fig. 19.

Because some parameters of GaN are unknown at present, the theoretical predictions of the binding energy and the Fermi energy for EHL formation in GaN, based on the Beni & Rice method, have not yet been developed.

The band structure of GaN is very similar to those of CdS and ZnS. So we can estimate the values of the binding

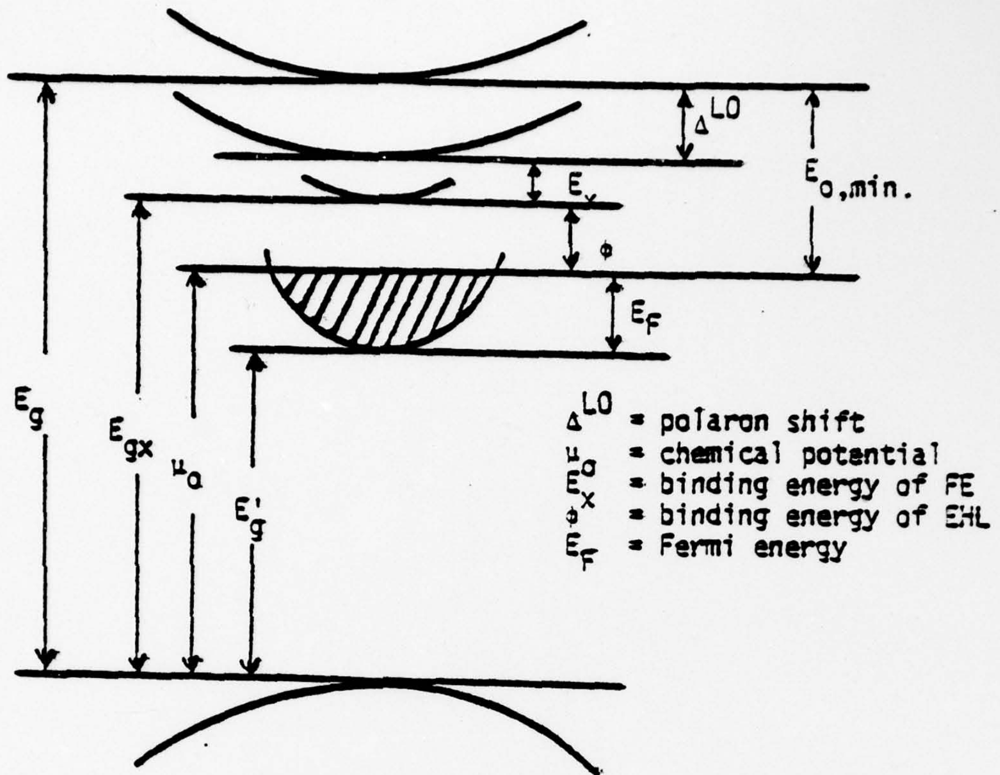

(a) Theoretical prediction: $\phi = \Delta^{LO} - E_x - E_{o,min.}$

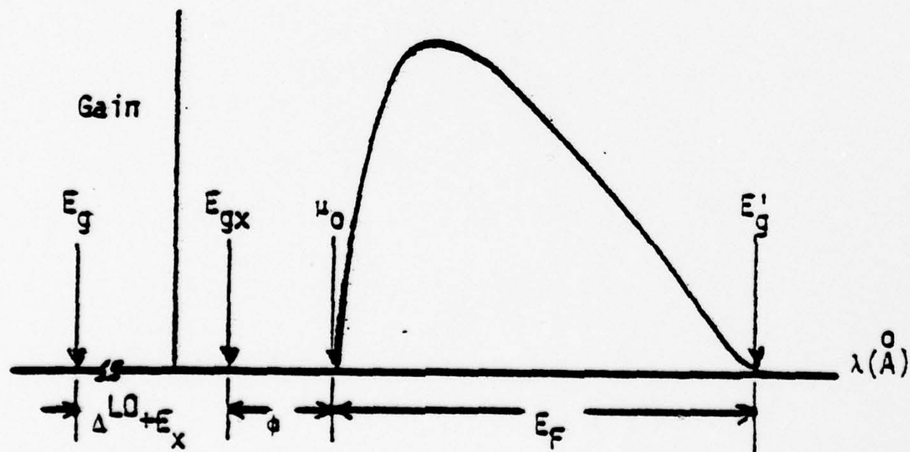

(b) Experimental data: $\phi = E_{gx} - \mu_o$

Fig. 19 Determination of the EHL binding energy from the theoretical prediction and the experimental gain spectrum.

energy ψ (~7-13 meV), the liquid density n_o (~4-5 x 10^{18} cm^{-3}), the critical density n_c (~0.8-1.4 x 10^{18} cm^{-3}), and the critical temperature T_c (~80°K).

C. EHL Model In GaN

Our data can be best described by an EHL bound by 10 meV with a Fermi energy of 55 meV.

In Fig. 18 the energy difference between the high-energy edge of the gain spectra and the free-exciton energy, corresponding to the EHL binding energy, is given as:

$$\psi\ (\text{EHL}) = 3.477\ \text{eV}\ (3565\ \text{Å}) - 3.467\ \text{eV}\ (3575\ \text{Å})$$
$$= 10\ \text{meV} \quad @\ 4.2^\circ\text{K}$$

At 0°K the gain linewidth corresponds to the sum of the carrier Fermi energies. This is directly related to the carrier density n_o within the EHL drop. At high temperatures, the thermal excitation of the Fermi system modifies the distribution of carriers, but the gain linewidth is still equal to the sum of the carrier Fermi energies. The gain spectra of GaN at 77°K for different pump power densities P(%) are shown in Fig. 20 . Here the gain linewidths are significantly reduced with decreasing pump power density, but their half-widths (FWHM) of remain almost constant.

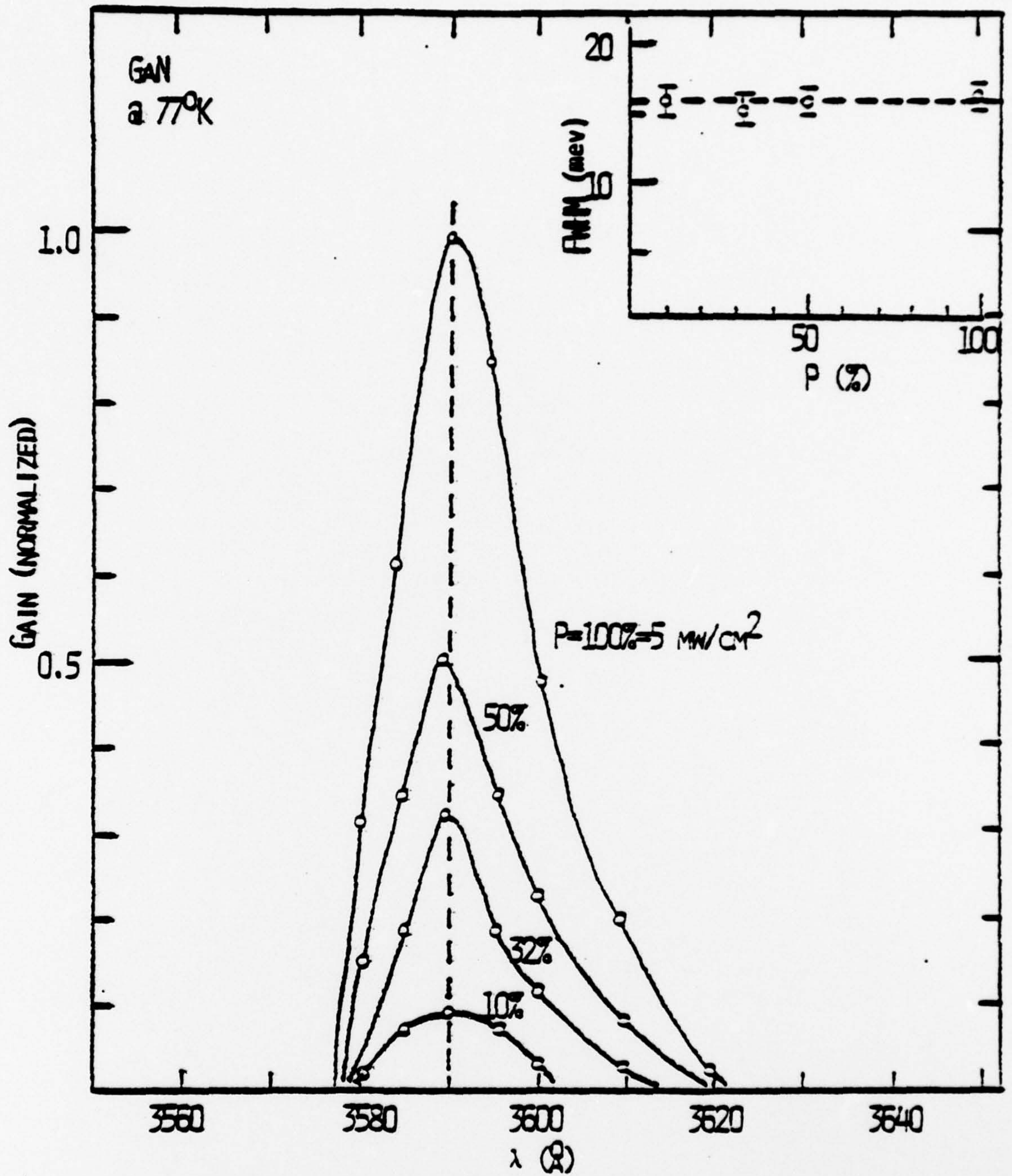

Fig. 20 Gain spectra of GaN at 77°K for different pump power density

For GaN, the combined Fermi energy of electrons and holes at $T = 0^oK$ is

$$E_F(0) = E_F^e + E_F^h = \frac{\hbar^2}{2}\left(\frac{1}{m_e^*} + \frac{1}{m_h^*}\right) (3\pi^2 n_o)^{2/3} \tag{16}$$

where $m_e^* = 0.2\ m_o$

$$m_h^* = (m_{h,//} m_{h,\perp}^2)^{1/3} = (5 \times 0.8^2)^{1/3} = 1.48\ m_o$$

Thus,

$$E_F(0) = 2.05 \times 10^{-11}\ n_o^{\ 2/3} \tag{17}$$

From this equation, we can estimate the expected linewidth for a plasma having an average density $\bar{N}$ corresponding to the excitation density, assuming the carrier lifetime to be 10^{-10} sec and the excitation penetration depth of about 10^{-5} cm.

It is clear that the measured linewidth at 4.2^oK is independent of the pump intensity, and is much broader at low pump intensity than expected for a simple plasma with density $\bar{N}(cm^{-3})$ as shown in Fig. 21. The data of linewidth 55 meV are best fitted with a fixed density $n_o = 4.4 \times 10^{18}$ cm^{-3} which is the carrier density within the drop at $T = 0^oK$. At 77^oK the measured linewidth drops rapidly as the pump intensity is decreased.

The Fermi energy E_F is assumed to be fixed, consistent with a constant value of n_o. Strictly speaking this is true only at $T = 0^oK$. For finite temperatures, a correction to

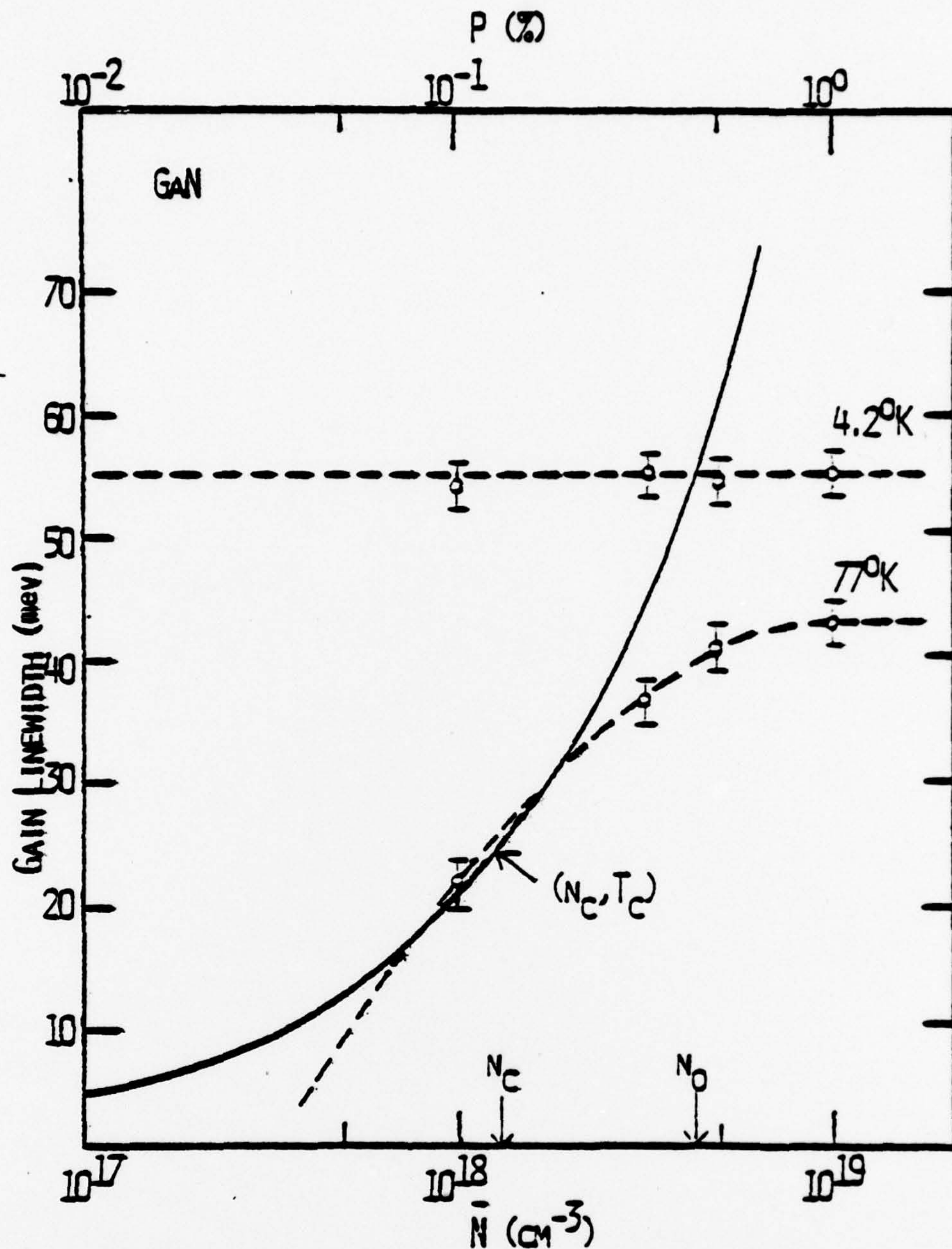

Fig. 21 VARIATION OF GAIN LINEWIDTH WITH THE PUMP POWER DENSITY. THE DASHED CURVES ARE EXPERIMENTAL DATA AT 4.2°K AND 77°K. THE SOLID CURVE IS THE EXPECTED LINEWIDTH FOR A PLASMA WITH AN AVERAGE DENSITY $\bar{N}$.

the Fermi energy is necessary due to the variation of E_F with temperature at constant density, and also due to the change of n itself with temperature since n(T) itself is determined by minimizing the total free energy F of the system.

For the case where $\tilde{N} > n_o$ ($\tilde{N} = 10^{19}$ cm^{-3}) the pump laser can generate an excitation density greater than the liquid density and we observe less temperature variation of the gain linewidth. In this case, the observed reduction of linewidth with temperature can be determined by calculating the thermal variation of the sum of the electron and hole Fermi energies for constant carrier density, i.e. n(T) = const. = n_o. The correction to E_F with temperature for constant density n_o is well-known from statistical mechanics. This is equivalent to the familiar Sommerfeld term $-\pi^2(k_BT)^2/12E_F$ for a free electron gas, and is given by

$$\delta E_F(T) = -\frac{\pi^2}{12} \frac{(k_BT)^2}{E_F^e(0)\ E_F^h(0)} E_F(0) \tag{18}$$

It is shown by the dashed curve in Fig. 22.

For the case where $\tilde{N} < n_o$, the correction to E_F due to variation of n(T) with temperature is a more important correction and can be evaluated from thermodynamics, i.e., the

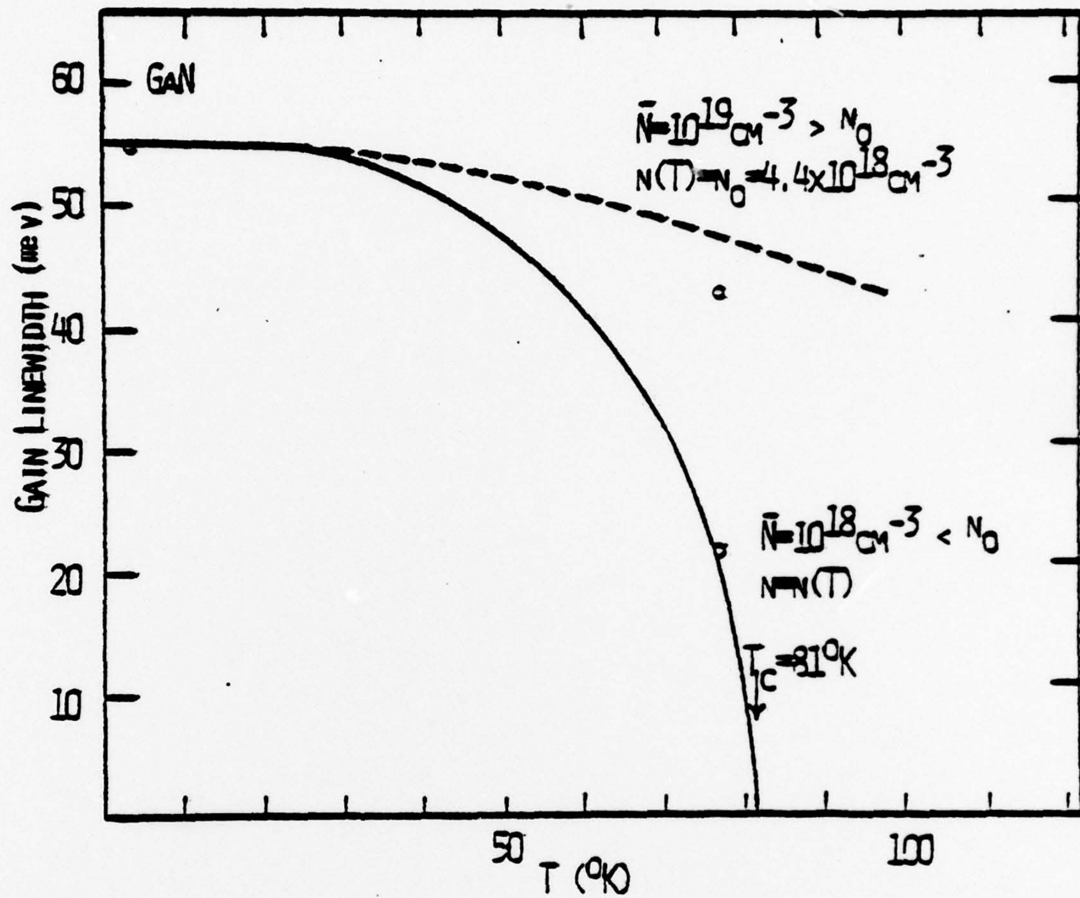

Fig. 22 VARIATION OF GAIN LINEWIDTH WITH TEMPERATURE. THE CIRCLES ARE EXPERIMENTAL DATA. THE DASHED CURVE IS CALCULATED BY THE VARIATION OF CONSTANT DENSITY FERMI LIQUID, AND THE SOLID CURVE IS THE PHASE DIAGRAM.

thermal expansion of the e-h liquid. We can write an expansion to secondorder in T for the free energy per pair F of the EHL using the Landau theory of the Fermi liquid.

$$F(n,T) = E_0(n) - \tfrac{1}{2}\gamma(n)(k_B T)^2 \tag{19}$$

where $E_0(n)$ is the ground-state energy per pair as a function of e-h pair density in the drop. The second term essentially corresponds to an entropy contribution -TS with the entropy linear in temperature, $S = \gamma T$, characteristic of a metal. The coefficient $\gamma(n)$ is given by

$$\gamma(n) = \frac{1}{\hbar^2}\left(\frac{\pi}{3n}\right)^{2/3}(m_{de} + m_{dh}) \tag{20}$$

Equation (19) can be expanded to second order about the equilibrium density n_0,

$$F(n,T) = E_0(n_0) + \tfrac{1}{2}E''_0(n-n_0)^2 - \tfrac{1}{2}\gamma(n)(k_B T)^2 \tag{21}$$

where primes denote derivatives w.r.t. n evaluated at n_0. By minimizing $F(n,T)$ in equation (21):

$$E'_0 = 0 \text{ at } n = n_0$$

$$\delta F/\delta n = 0 = E''_0(n-n_0) - \tfrac{1}{2}\gamma'(n)(k_B T)^2 \tag{22}$$

The variation of density with temperature is then:

$$n(T) = n_0 + \frac{\tfrac{1}{2}\gamma'(n)}{E''_0}(k_B T)^2 \tag{23}$$

By combining Equations (18) and (23), it can be seen that the Fermi energy $E_F(T)$ at arbitrary T is

$$E_F(T) = E_F(0)\ (1 - \frac{\pi^2}{12} \frac{(k_B T)^2}{E_F^e\ E_F^h} + \frac{\gamma'(n)\ (k_B T)^2}{3\ n_o\ E_o''} \quad (24)$$

For convenience in discussing the experimental data we introduce the prefactors δ_n and δ_E according to

$$n(T) = n_o(1 - \delta_n(k_B T)^2) \quad (25)$$

$$E_F(T) = E_F(0)\ (1 - \delta_E(k_B T)^2) \quad (26)$$

Finally, we can estimate the value of δ_n and δ_E:

$$\delta_n = 0.0145 \pm 0.0015\ (mev)^{-2}$$

$$\delta_E = 0.0136 \pm 0.0005\ (mev)^{-2}$$

Now, we can estimate the critical temperature using the equation as follows:

$$n_c(T_c) = n_o\ (1 - \delta_n(k_B T_c)^2) \quad (27)$$

where n_c is graphically estimated by the value of 1.3×10^{18} cm^{-3}, which is indicated by the arrow-head in Fig. 21. Therefore, the critical temperature T_c can be determined from Equation (27) to be 81^oK. The liquid-gas coexistence curve in the phase diagram of GaN is shown by the plot of T/T_c vs. n/n_o in Fig. 23.

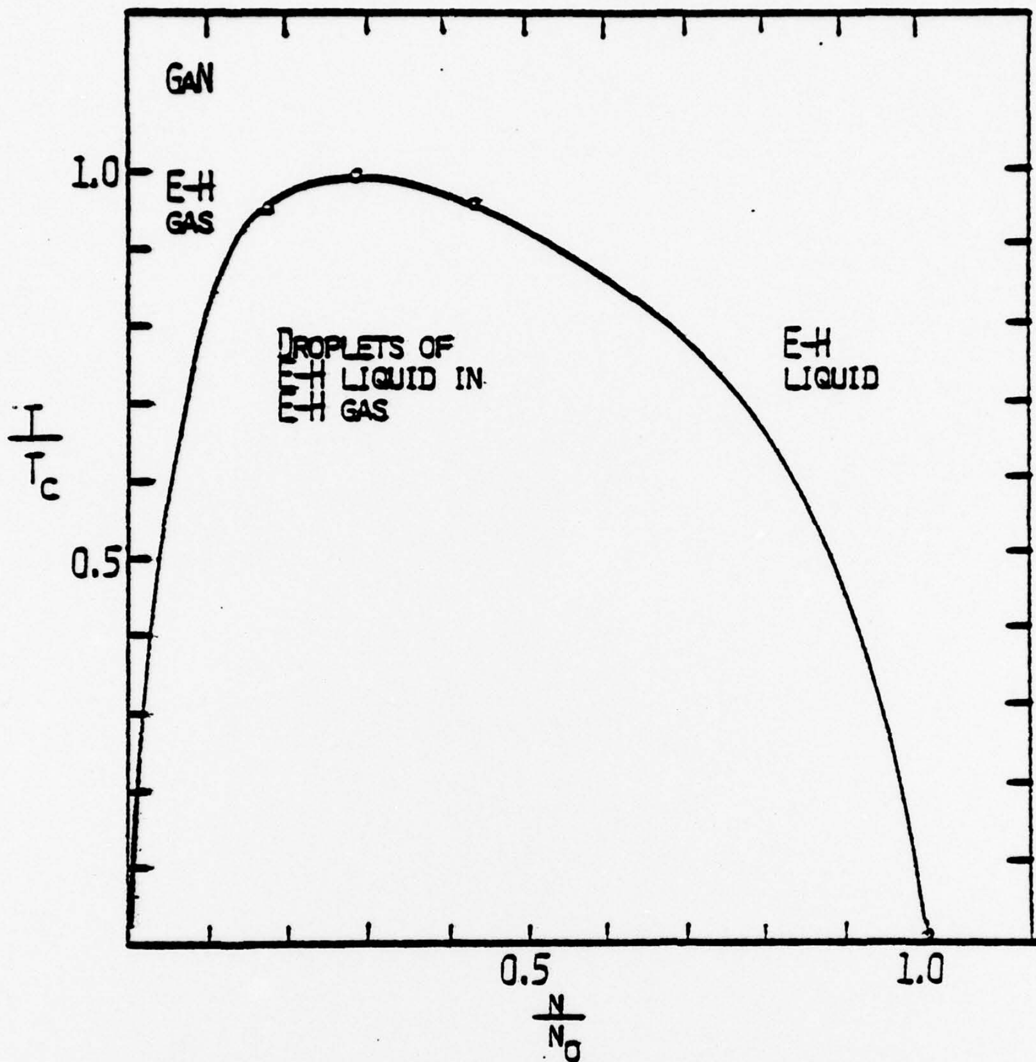

Fig. 23 THE EXPECTED LIQUID-GAS COEXISTENCE CURVE IN THE PHASE DIAGRAM OF GaN. THE CIRCLES ARE EXPERIMENTAL DATA.

In conclusion, by analyzing the spectral and temperature dependence of the laser transition we deduce that it is due to electron-hole-liquid recombination. It is identified here for the first time in GaN, a relatively polar semiconductor. A binding energy of 10 meV, a very high critical temperature of 81°K, and a low temperature liquid density of 4.4×10^{18} cm^{-3} are deduced and provide strong evidence for the proposed mechanism of the transition.

REFERENCES

1. J. I. Pankove, H. P. Maruska, and J. E. Berkeyheiser, Internat. Semicond. Conf., Boston, 1970.
2. R. Dingle, K. L. Shaklee, R. F. Leheny, and R. B. Zetterstrom, Appl. Phys. Lett., 19, 5 (1971).
3. K. L. Shaklee and R. F. Leheney, Appl. Phys. Lett., 18, 475 (1971).
4. R. Dingle, D. D. Sell, S. E. Stokowski, and M. Ilegems, Phys. Rev., B 4, 1211 (1971).
5. J. M. Hvam and E. Ejder, J. Lumin., 12/13, 611 (1976).
6. T. M. Rice, "Proc. XII. Internat. Conf. Phys. Semicond.," p. 23, Stuttgart, 1974.
7. W. F. Brinkman and T. M. Rice, Phys. Rev., B 7, 1508 (1973).
8. G. Beni and T. M. Rice, Phys. Rev. Lett., 37, 874 (1976).
9. L. V. Keldysh and A. P. Silin, Sov. Phys. JETP 42, 535 (1976).
10. M. Rösler and R. Zimmerman, Phys. Stat. Sol. (b) 83, 85 (1977).
11. R. F. Leheny and J. Shah, Phys. Rev. Lett., 37, 871 (1976).
12. R. F. Leheny and J. Shah, Phys. Rev. Lett., 38, 511 (1977).
13. G. O. Müller, H. H. Weber, V. G. Lysenko, V. I. Revenko, and V. B. Timofeev, Solid State Commun., 21, 217 (1977).
14. V. G. Lysenko, V. I. Revenko, T. G. Tratas, and V. B. Timofeev, Sov. Phys. JETP 41, 163 (1975).
15. O. Hildebrand, B. O. Faltermeier, and M. H. Pilkuhn, Solid State Commun., 19, 841 (1976).

16. D. Hulin, A. Mysyrowicz, M. Combescot, I. Pelant, and C. Benoit a la Guillaume, Phys. Rev. Lett., 39, 1169 (1977).

17. K. L. Shaklee, R. E. Nahory, and R. F. Leheny, J. Lumin., 7, 284 (1974).

DISTRIBUTION LIST

Contract N00014-75-C-0295

Address	Copies
Chief of Naval Research Attn: Code 427 Arlington, VA 22217	3 copies
Chief of Naval Research Attn: Code 105 Arlington, VA 22217	6 copies
Director Naval Research Laboratory Washington, DC 20375 Attn: Code 2627 5220	 6 copies 1 copy
Defense Documentation Center Building 5 Cameron Station Alexandria, VA 22314	12 copies*
Advisory Group on Electron Devices 9th floor 201 Varick Street New York, NY 10014	1 copy
Texas Instruments, Inc. P. O. Box 5012 Dallas, TX 75222 Attn: Dr. Robert W. Haisty	1 copy
University of Southern California School of Engineering Department of Materials Science University Park Los Angeles, CA 90007 Attn: Professor M. Gershenzon	1 copy
Office of the Director of Defense Research and Engineering Information Office Library Branch The Pentagon Washington, DC 20301	1 copy
U.S. Army Research Office Box CM, Duke Station Durham, NC 27706	1 copy
Director, National Bureau of Standards Attn: Technical Library Washington, DC 20234	1 copy

* to be submitted with a completed DDC Form 50

Enclosure (3)

Commanding Officer
Office of Naval Research Branch Office
536 Clark Street
Chicago, IL 60605 — 1 copy

Air Force Cambridge Research Laboratory
L.G. Hanscom Field
Technical Library
Cambridge, MA 02138 — 1 copy

Harry Diamond Laboratories
2800 Powder Mill Road
Adelphia, MD 20783
Attn: Technical Library — 1 copy

Commandant, Marine Corps
Scientific Advisor (Code AX)
Washington, DC 20380 — 1 copy

Naval Missile Center
Technical Library (Code 5632.2)
Point Mugu, CA 93010 — 1 copy

Naval Ocean Systems Center
Code 922/H. Wieder
San Diego, CA 92152 — 1 copy

Naval Weapons Laboratory
Technical Library
Dahlgren, VA 22448 — 1 copy

North Carolina State University
Electrical Engineering Department
Attn: Professor M. A. Littlejohn
Raleigh, NC 27607 — 1 copy

RCA Laboratories
David Sarnoff Research Center
Princeton, NJ 08540
Attn: Dr. Y. Narayan — 1 copy
Dr. J. Pankove — 1 copy

Raytheon Company
Research Division
28 Seyon Street
Waltham, MA 02154 — 1 copy

Naval Avionics Facility
Technical Library
Indianapolis, IN 46218 — 1 copy

Air Force Office of Scientific Research — 1 copy
Department of the Air Force
Bolling Air Force Base
Washington, DC 20332

Commanding Officer — 1 copy
Office of Naval Research Branch Office
1030 East Green Street
Pasadena, CA 91101

Director — 1 copy
U.S. Army Engineering Research and
Development Laboratories
Fort Belvoir, VA 22060
Attn: Technical Documents Center

Air Force Avionics Laboratory — 1 copy
Air Force Systems Command
Technical Library
Wright-Patterson Air Force Base
Dayton, OH 45433

Director — 1 copy
Defense Advanced Research
Projects Agency
Attn: Technical Library
1400 Wilson Boulevard
Arlington, VA 22209

Naval Air Systems Command — 1 copy
Air - 310/J. Willis
Washington, DC 20361

Stanford University — 1 copy
Attn: Professor W. Tiller
Department of Materials Science
and Engineering
Stanford, CA 94305

Bell Telephone Labs — 1 copy
Attn: R. Dingle
Murray Hill, NJ 07974

North Carolina State University — 1 copy
2205 Hillsbourogh
Electrical Engineering
Attn: Professor M. A. Littlejohn
Raleigh, North Carolina 27607